Hamburger Beiträge
zur Angewandten Mathematik

Asymptotic based preconditioning technique for low Mach number flows

A. Meister

Reihe F
Computational Fluid Dynamics and Data Analysis 15
August 2001

Hamburger Beiträge zur Angewandten Mathematik

Reihe A	Preprints
Reihe B	Berichte
Reihe C	Mathematische Modelle und Simulation
Reihe D	Elektrische Netzwerke und Bauelemente
Reihe E	Scientific Computing
Reihe F	Computational Fluid Dynamics and Data Analysis

Meister, A.

Asymptotic based preconditioning technique for low Mach number flows

A comprehensive study of a finite volume method for inviscid flow fields at high and low speeds is presented. Thereby, the results of a formal single as well as multiple scale asymptotic low Mach number analysis [34, 45] of the Euler equations of gas dynamics are used to extend the validity of the numerical method from the simulation of compressible inviscid flow fields to the low Mach number regime. Although different strategies are applicable [28, 35, 34, 47] we focus our view to a preconditioning technique proposed by Guillard and Viozat [14]. After a brief repetition of an asymptotic analysis in the continuous context we present a finite volume approximation of the governing equations using the AUSMDV scheme [77]. To overcome the failure of the original approach in the low Mach number regime we combine the numerical flux function with a preconditioned formulation of the Lax-Friedrichs scheme. Both, a wide variety of trans-, super-, hyper-, and subsonic realistic test cases and a formal discrete asymptotic single scale analysis are employed in order to prove the validity of the derived numerical method from hypersonic to low Mach number fluid flow.

1. Introduction

Flow fields in fluid mechanics are subdivided into compressible and incompressible flows. The decomposition is usually based on the Mach number representing the quotient of the flow velocity and the speed of sound. Compressible inviscid fluid flow of an ideal gas is modeled by the Euler equations of gas dynamics which is a typical representative of a hyperbolic system of partial differential equations and the incorporated pressure is determined by an algebraic equation of state. On the other hand, within the incompressible Euler equations the pressure takes the role of a Lagrangian multiplier such that the velocity field satisfies an elliptic divergence constraint.

Although the equations are of different type there is no exact dividing line between the compressible and incompressible regime. For example, the flow in a nozzle often shows large compressible as well as incompressible regions. Furthermore, a laminar combustion with a Mach number between 10^{-4} and 10^{-3} can be accelerated by external or self-induced forces in such a way that a fast transition from deflagration to detonation takes place and drives the flow field towards a complete compressible regime where the Mach number grows to values between 5 and 10.

Obviously, current flow solvers which are based on the equations of either compressible or incompressible fluid flow are usually not suitable to simulate flow fields of varying type except when the transition between both regimes is handled in a physical senseful manner. Briley et. al. [5] and Merkle et. al. [52] reported of performance and accuracy problems in the case that standard compressible methods are used for the simulation of low Mach number flows. Sesterhenn [61] investigated this phenomenon with the view on rounding errors, Volpe [76] described the influence of mesh adaption and Hauke et. al. [20] studied the effects of using different sets of variables. All these and several further research activities show that the extension of a compressible solver to the incompressible regime and vice versa requires an appropriate mathematical analysis of the governing equations in order to extract the main features of the physical quantities in the limit of interest. Asymptotic expansions represent one of the most powerful and efficient tools in the backbone of such assignments and are widely used in almost all areas of science to get a deeper insight into the behaviour of solutions of partial differential equations [8, 31, 60]. Concerning the Euler equations, Klainerman and Majda [32, 33] investigated the zero Mach number limit of the equations of compressible ideal fluid flow. In their study the fluid was assumed to be barotropic and a single scale asymptotic expansion was used. Hence acoustic effects were neglected in their investigation. Asano [2] and Ukai [72] improved the results in the sense that weaker assumptions on the initial conditions are considered. In particular, the divergence free condition of the initial data was removed. In [34, 45] a single time scale, multiple length scale asymptotic analysis of the compressible Euler equations is employed in order to investigate the behaviour of the fluid flow in the low Mach number regime. Thereby the conservative formulation of the Euler equations is considered and the results are used to extend the validity of a numerical method from the compressible to the low Mach number regime by the introduction of multiple pressure variables, whereby acoustic effects as well as variable density distributions are taken into account [34]. The validity of such a numerical method strongly depends on the choice of the asymptotic sequence which has to represent a measure of the compressibility of the fluid as well as the physically based decomposition of the pressure field. Therefore, in [26, 27, 28, 47, 25] an algorithm is developed for the simultaneous computation of the Mach number

and the associated pressure decomposition from a given discrete flow field. The method is based on algorithms from image processing [39, 38] and introduced in a numerical method closely connected to those presented in [34, 59]. A comprehensive survey on asymptotic methods can be found in [35].

Guillard and Viozat [14] preconditioned the numerical dissipation within the Riemann-solver of Roe. Thereby, a discrete asymptotic single scale analysis is employed to prove the validity of this slightly modified Roe method in the low Mach number regime. This procedure overcomes the disadvantage of standard preconditioning techniques [53, 71, 6] which usually restricts the underlying numerical method to the simulation of steady flow fields except for the case that the scheme is involved in a dual time stepping environment [63, 79, 75].

The paper deals with the extension of the validity of a standard finite volume scheme for the solution of compressible flow fields to the low Mach number regime. The aims are to prove the unphysical behaviour of the AUSMDV method proposed by Liou and Wada [77] and to combine this algorithm with a modified Lax-Friedrichs scheme in order to overcome this failure. The modification is based on a simple preconditioning technique recently suggested by Guillard and Viozat [14].

The outline of this paper is as follows. In Chapter 2 we summarize the results of a formal asymptotic single as well as multiple scale analysis of the governing equations to emphasize the behaviour of the physical quantities. Special attention is laid on the reference parameters employed within the non-dimensionalization and the distribution of the leading as well as first order pressure term. Chapter 3 is devoted to the description of a finite volume method on unstructured grids. The scheme was originally proposed by Sonar and it is developed in a large number of publications [64, 19, 22, 11, 50, 42, 43, 44]. The accuracy of the method is discussed in the context of different well known and realistic test cases from fluid mechanics. Similar to the continuous case a formal discrete asymptotic expansion is introduced to study the behaviour of the numerical pressure distribution in the case of low Mach number flows. The statements of the mathematical theory concerning the failure of the standard compressible finite volume method are confirmed by flow simulations about the RAE2822 airfoil at different freestream Mach numbers. Considering the system of perturbation equations arising within the asymptotic analysis of the numerical method one can additionally get detailed hints concerning a modification of the scheme in order to satisfy the continuous properties of the pressure field in a discrete sense. Motivated by the asymptotic results a preconditioning matrix is described in Chapter 4 and employed to correct the numerical dissipation of the scheme. The physically senseful properties of the preconditioned approach are proved by means of the discrete asymptotic analysis and they are confirmed by numerical experiments. Finally, we close with a brief outlook and some concluding remarks.

2. Governing equations

The equations governing time-dependent inviscid flow are called the Euler equations of gas dynamics. This hyperbolic system of partial differential equations represents the natural form of the fundamental laws of conservation of mass, momentum and energy. With respect to the spatial domain $G \subset \mathbb{R}^2$ which is assumed to be polygonally bounded by $\partial G = \bigcup_{k=1,\dots,n} \partial G_k$, the conservative form of the governing equations writes

$$\partial_{\hat{t}} \hat{\mathbf{u}} + \sum_{\ell=1}^{2} \partial_{\hat{x}_\ell} \hat{\mathbf{f}}_\ell \left(\hat{\mathbf{u}} \right) = \hat{\mathbf{0}} \ \text{ in } \ G \times \mathbb{R}_0^+, \tag{1}$$

where

$$\hat{\mathbf{u}} = \begin{pmatrix} \hat{\rho} \\ \hat{\rho}\hat{v}_1 \\ \hat{\rho}\hat{v}_2 \\ \hat{\rho}\hat{E} \end{pmatrix}$$

and

$$\hat{\mathbf{f}}_\ell \left(\hat{\mathbf{u}} \right) = \begin{pmatrix} \hat{\rho}\hat{v}_\ell \\ \hat{\rho}\hat{v}_1\hat{v}_\ell + \delta_1^\ell \hat{p} \\ \hat{\rho}\hat{v}_2\hat{v}_\ell + \delta_2^\ell \hat{p} \\ \hat{\rho}\hat{H}\hat{v}_\ell \end{pmatrix}$$

denote the vector of conserved variables and the convective fluxes, respectively. Herein $\hat{\rho}$, $\hat{v}_\ell$, $\hat{m}_\ell = \hat{\rho}\hat{v}_\ell$, $\hat{p}$, $\hat{E}$, $\hat{H} = \hat{E} + \hat{p}/\hat{\rho}$ describe density, velocity and momentum in x_ℓ-direction, pressure, total energy and enthalpy of the

fluid, respectively. Furthermore δ_i^ℓ denotes the Kronecker symbol. In order to close the system an equation of state is needed which can be expressed as

$$\hat{p} = (\gamma - 1)\,\hat{\rho}\left(\hat{E} - \frac{|\hat{\mathbf{v}}|^2}{2}\right) \tag{2}$$

with $\hat{\mathbf{v}} = (\hat{v}_1, \hat{v}_2)^T$. Here γ represents the ratio of specific heats which is assumed to be $\gamma = 1.4$ throughout the text. The system of Euler equations is to be solved under initial conditions

$$\hat{\mathbf{u}}(\hat{\mathbf{x}}, \hat{0}) = \hat{\mathbf{u}}_0(\hat{\mathbf{x}}), \quad \hat{\mathbf{x}} \in \overline{G},$$

as well as under boundary conditions

$$\hat{\mathbf{u}}(\hat{\mathbf{x}}, \hat{t}) = \hat{\mathbf{u}}_{\partial G_k}(\hat{t}), \quad \hat{t} \in \mathbb{R}^+, \quad \hat{\mathbf{x}} \in \partial G_k, \quad k = 1 \ldots, n.$$

In the context of compressible flow fields the non-dimensionalization of the Euler equations is usually performed by means of the reference values for length $\hat{x}_{ref}$, density $\hat{\rho}_{ref}$ and fluid velocity $\hat{v}_{ref}$ which are taken from the underlying physical flow field. The remaining reference values are determined via functional relationships like $\hat{p}_{ref} = \hat{\rho}_{ref}\hat{v}_{ref}^2$, $\hat{E}_{ref} = \hat{p}_{ref}/\hat{\rho}_{ref}$ and $\hat{t}_{ref} = \hat{v}_{ref}/\hat{x}_{ref}$. Introducing the expression

$$\hat{\varphi} = \varphi \cdot \hat{\varphi}_{ref}$$

for each physical quantity $\hat{\varphi}$ into the governing equations yields a non-dimensional formulation of the Euler equations which is identical to (1). Even the equation of state (2) remains unchanged.

In the case of a small velocity reference the definition of the pressure reference is no longer appropriate since it does not represent a sensible measure of the physical pressure field. In order to meet this fact we employ an independent pressure reference and hence the dimensionless form of the Euler equations and the equation of state become

$$\partial_t \underbrace{\begin{pmatrix} \rho \\ \rho v_1 \\ \rho v_2 \\ \rho E \end{pmatrix}}_{\mathbf{u} =} + \sum_{\ell=1}^{2} \partial_{x_\ell} \underbrace{\begin{pmatrix} \rho v_\ell \\ \rho v_1 v_\ell + \mathrm{M}^{-2}\delta_1^\ell p \\ \rho v_2 v_\ell + \mathrm{M}^{-2}\delta_2^\ell p \\ \rho H v_\ell \end{pmatrix}}_{\mathbf{f}_\ell(\mathbf{u}) =} = \mathbf{0} \tag{3}$$

and

$$p = (\gamma - 1)\,\rho\left(E - \frac{\mathrm{M}^2}{2}|\mathbf{v}|^2\right). \tag{4}$$

The non-dimensional characteristic number M appearing within (3) and (4) is called the Mach number which is defined as

$$\mathrm{M} = \frac{\hat{v}_{ref}}{\hat{c}_{ref}}$$

where $\hat{c}_{ref} = \sqrt{\hat{p}_{ref}/\hat{\rho}_{ref}}$ denotes the reference value for the speed of sound $\hat{c} = \sqrt{\gamma\hat{p}/\hat{\rho}}$. Based on this characteristic number we are now able to investigate the behaviour of the physical quantities in the low Mach number limit by means of a formal asymptotic analysis. Therefore, we assume throughout the paper that the non-dimensional formulation of the governing equations (3) consists exclusively of physical quantities φ satisfying $\varphi = O(1)$ if the Mach number tends to zero. We now briefly summarize only those statements of an asymptotic analysis which are important with respect to the investigation of the finite volume scheme presented in the following. For a comprehensive survey on the results of a single as well as multiple scale analysis we refer to [34, 45]. The success of an asymptotic analysis depends crucially on the choice of the incorporated asymptotic sequence $\{\phi_n(\mathrm{M})\}_{n\in\mathbb{N}_0}$ which in our case has to satisfy the assumption $\phi_n(\mathrm{M}) = o(\phi_{n-1}(\mathrm{M}))$, $\mathrm{M} \to 0$. The perturbation parameter within the governing equations (3) is the reciprocal value of the square of the Mach number. This seems to be the reason why many asymptotic expansions in the literature are based on the asymptotic sequence $\phi_n(\mathrm{M}) = \mathrm{M}^{2n}$. We employ the asymptotic sequence

$$\phi_n(\mathrm{M}) = \mathrm{M}^n, \quad n \in \mathbb{N}_0, \tag{5}$$

which is actually not obvious but several explanations concerning this choice will be given below. First, we focus our view on a formal single length scale, single time scale analysis. Therefore we assume that each physical quantity φ can be expressed in the form of an asymptotic expansion

$$\varphi(\mathbf{x},t;\mathrm{M}) = \sum_{m=0}^{j} \phi_m(\mathrm{M})\varphi^{(m)}(\mathbf{x},t) + o\left(\phi_j(\mathrm{M})\right), \quad \mathrm{M}\to 0, \quad j=0,1,2, \tag{6}$$

which is valid in $G\times\mathbb{R}_0^+$. Introducing the expansion (6) into the governing equations (3) with simultaneous consideration of the asymptotic sequence (5) yields an expression for the momentum equation of the form

$$\frac{1}{\mathrm{M}^2}\nabla_{\mathbf{x}}p^{(0)} + \frac{1}{\mathrm{M}}\nabla_{\mathbf{x}}p^{(1)} + \partial_t(\rho\mathbf{v})^{(0)} + \sum_{\ell=1}^{2}\partial_{x_\ell}(\rho v_\ell\mathbf{v})^{(0)} + \nabla_{\mathbf{x}}p^{(2)} = o(1), \quad \mathrm{M}\to 0. \tag{7}$$

Note that the so called asymptotic functions $\varphi^{(m)}$ do not depend on the Mach number M. Thus, we can identify terms multiplied by the same power of M. Consequently, we obtain the following perturbation equations

$$\nabla_{\mathbf{x}}p^{(0)} = \mathbf{0} \ \text{ and } \ \nabla_{\mathbf{x}}p^{(1)} = \mathbf{0},$$

which directly prove that the pressure field becomes

$$p(\mathbf{x},t;\mathrm{M}) = p^{(0)}(t) + \mathrm{M}p^{(1)}(t) + \mathrm{M}^2p^{(2)}(\mathbf{x},t) + o\left(\mathrm{M}^2\right), \quad \mathrm{M}\to 0. \tag{8}$$

This result shows that the maximal influence of spatial fluctuations inside the pressure distribution are of order $O(\mathrm{M}^2)$ whereas $O(1)$-variations can only appear in the temporal evolution uniformly in G.

Taking into account the characteristic wave speeds in direction $\mathbf{n}$

$$v_{\mathbf{n}} = O(1), \quad \mathrm{M}\to 0, \quad \text{and} \quad v_{\mathbf{n}} \pm \frac{c}{\mathrm{M}} = O\left(\frac{1}{\mathrm{M}}\right), \quad \mathrm{M}\to 0,$$

it is obvious that the propagation of information is associated with two different length scales, namely

$$\eta = \mathbf{x} \ \text{ and } \ \xi = \mathrm{M}\mathbf{x}.$$

This observation motivates the consideration of multiple length scale asymptotic expansions and gives a first hint concerning the use of the asymptotic sequence (5) mentioned above. The investigation of the multiple scales requires some additional mathematical assumptions which we now briefly introduce. A precise description can be found in [45, 47]. In order to enable the existence of long wave length phenomena on the scale $\xi = \mathrm{M}\mathbf{x}$ the spatial domain is assumed to be large enough such that these effects are always possible. Corresponding to the single length scale case we consider solutions $\mathbf{u}$ of the Euler equations (3) where each physical quantity φ can be expressed by an asymptotic expansion

$$\varphi(\mathbf{x},t;\mathrm{M}) = \sum_{m=0}^{j} \phi_m(\mathrm{M})\varphi^{(m)}\left(\mathbf{g}(\mathbf{x},t;\mathrm{M})\right) + o\left(\phi_j(\mathrm{M})\right), \quad \mathrm{M}\to 0, \quad j=0,1,2, \tag{9}$$

which is valid in $G\times\mathbb{R}_0^+$. Thereby, the influence of multiple length scales is performed via the mapping $\mathbf{g}$ which is determined as

$$\begin{array}{rcl} \mathbf{g}:\mathbb{R}^2\times\mathbb{R}_0^+\times(0,\widetilde{\mathrm{M}}) & \longrightarrow & \mathbb{R}^2\times\mathbb{R}^2\times\mathbb{R}_0^+ \\ (\mathbf{x},t;\mathrm{M}) & \overset{\mathbf{g}}{\longmapsto} & (\mathbf{x},\mathrm{M}\mathbf{x},t), \end{array}$$

where $1 \gg \widetilde{\mathrm{M}} > 0$. Consequently, the asymptotic functions are given by

$$\begin{array}{rcl} \varphi^{(m)}:\mathbb{R}^2\times\mathbb{R}^2\times\mathbb{R}_0^+ & \longrightarrow & \mathbb{R}, \quad m=0,1,2 \\ (\eta,\xi,t) & \overset{\varphi^{(m)}}{\longmapsto} & \varphi^{(m)}(\eta,\xi,t). \end{array}$$

It is proved in [45] that the asymptotic functions $\varphi^{(m)}$, $m=1,2$, satisfy the so called sublinear growth condition

$$\varphi^{(m)}\left(\mathbf{g}(\mathbf{x},t;\mathrm{M})\right) = o(|\mathbf{x}|), \quad \mathbf{x}\in\partial B_{\mathbf{x}}\left(\frac{1}{\mathrm{M}}\right), \quad \mathrm{M}\to 0, \quad m=1,2, \tag{10}$$

if the asymptotic expansion (9) is uniformly valid outside an arbitrarily large ball

$$B_{\mathbf{x}}(s) = \left\{ \mathbf{x} \in \mathbb{R}^2 \,\middle|\, |\mathbf{x}| < s \right\}, \quad s \in \mathbb{R}^+.$$

The main proceeding is now equivalent to the single length scale case whereby some additional mathematical assumptions have to be introduced due to the dependence of the asymptotic functions $\varphi^{(i)}$ on the Mach number M. In order to develop the basic ideas we suppose that the following steps are admissible. A comprehensive mathematical framework is elaborated in [45, 47]. Introducing the asymptotic expansion (9) into the governing equations (3) and using the derivatives

$$\partial_t \left(\varphi^{(m)} \circ \mathbf{g} \right) (\mathbf{x}, t; \mathrm{M}) = \partial_t \varphi^{(m)} \left(\mathbf{g}(\mathbf{x}, t; \mathrm{M}) \right)$$

and

$$\partial_{x_j} \left(\varphi^{(m)} \circ \mathbf{g} \right) (\mathbf{x}, t; \mathrm{M}) = \partial_{\eta_j} \varphi^{(m)} \left(\mathbf{g}(\mathbf{x}, t; \mathrm{M}) \right) + \mathrm{M} \partial_{\xi_j} \varphi^{(m)} \left(\mathbf{g}(\mathbf{x}, t; \mathrm{M}) \right), \quad j = 1, 2,$$

we obtain from the momentum equation

$$\frac{1}{\mathrm{M}^2} \nabla_\eta p^{(0)} + \frac{1}{\mathrm{M}} \left(\nabla_\xi p^{(0)} + \nabla_\eta p^{(1)} \right) = o\left(\frac{1}{\mathrm{M}} \right), \quad \mathrm{M} \to 0.$$

The implications for the momentum balance of order $\frac{1}{\mathrm{M}^2}$ and $\frac{1}{\mathrm{M}}$ are

$$\nabla_\eta p^{(0)} = \mathbf{0} \tag{11}$$

and

$$\nabla_\xi p^{(0)} = -\nabla_\eta p^{(1)}. \tag{12}$$

As a first statement we obtain directly from (11)

$$p^{(0)} = p^{(0)}(\xi, t). \tag{13}$$

Exploring the behaviour of the first order pressure term $p^{(1)}$ by integrating equation (12) over the open ball $B_\eta\left(\frac{1}{\mathrm{M}}\right)$ yields

$$\begin{aligned}
\nabla_\xi p^{(0)} &\overset{(13)}{=} \frac{1}{\left| B_\eta\left(\frac{1}{\mathrm{M}}\right) \right|} \int_{B_\eta\left(\frac{1}{\mathrm{M}}\right)} \nabla_\xi p^{(0)} \, d\eta \overset{(12)}{=} -\frac{1}{\left| B_\eta\left(\frac{1}{\mathrm{M}}\right) \right|} \int_{B_\eta\left(\frac{1}{\mathrm{M}}\right)} \nabla_\eta p^{(1)} \, d\eta \\
&= -\frac{1}{\left| B_\eta\left(\frac{1}{\mathrm{M}}\right) \right|} \int_{\partial B_\eta\left(\frac{1}{\mathrm{M}}\right)} p^{(1)} \cdot \mathbf{n} \, ds \overset{(10)}{=} O\left(\mathrm{M}^2\right) O\left(\frac{1}{\mathrm{M}}\right) o\left(\frac{1}{\mathrm{M}}\right) \\
&= o(1), \quad \mathrm{M} \to 0.
\end{aligned}$$

Hence the leading order pressure field fulfills $p^{(0)} = p^{(0)}(t)$ and it follows straightforwardly from the first order momentum equation (12) that the spatial variations within the first order pressure term $p^{(1)}$ can appear at most on the long wave scale ξ. These statements can be summarized in the important result

$$p(\mathbf{x}, t; \mathrm{M}) = p^{(0)}(t) + \mathrm{M} p^{(1)}(\xi, t) + \mathrm{M}^2 p^{(2)}(\eta, \xi, t) + o\left(\mathrm{M}^2\right), \quad \mathrm{M} \to 0. \tag{14}$$

In order to supply a measure concerning the comparison between the analytical and numerical pressure distribution we introduce the indicator

$$\mathrm{Ind}(p) = \begin{cases} \dfrac{p_{\max} - p_{\min}}{p_{\max} \, \Delta \mathbf{x}_p} & \text{if } p_{\max} \neq p_{\min}, \\ 0 & \text{otherwise}, \end{cases} \tag{15}$$

where $p_{\max}$, $p_{\min}$, $\Delta \mathbf{x}_p$ denote the maximal and minimal pressure value and the minimal spatial distance between $p_{\max}$ and $p_{\min}$ with respect to the Euclidean norm, respectively.

In the context of the single length scale asymptotic analysis the expression (8) directly proves

$$\mathrm{Ind}(p) = O\left(\mathrm{M}^2\right), \quad \mathrm{M} \to 0. \tag{16}$$

With respect to the multiple length scale expansion we distinguish two different cases. If the first order pressure field is spatially constant then the expansion (14) degenerates to the single scale expression (8) and consequently $\mathrm{Ind}(p) = O\left(\mathrm{M}^2\right)$, $\mathrm{M} \to 0$, follows. In the case of a spatially varying first order pressure field $p^{(1)}$ we conclude $p_{\max} - p_{\min} = O\left(\mathrm{M}\right)$, $\mathrm{M} \to 0$. Due to the fact that spatial variations within $p^{(1)}$ are associated with the length scale ξ we obtain $\frac{1}{\Delta \mathbf{x}_p} = O\left(\mathrm{M}\right)$, $\mathrm{M} \to 0$, which proves

$$\mathrm{Ind}(p) = O\left(\mathrm{M}^2\right), \quad \mathrm{M} \to 0, \tag{17}$$

also in the multiple length scale case.

3. Finite volume method

In order to rewrite the Euler equations in a convenient manner for standard compressible flow solvers we define the auxiliary variables

$$\widetilde{p} = \frac{p}{\mathrm{M}^2}, \quad \widetilde{c} = \frac{c}{\mathrm{M}}, \quad \widetilde{E} = \frac{E}{\mathrm{M}^2} \quad \text{and} \quad \widetilde{H} = \frac{H}{\mathrm{M}^2}. \tag{18}$$

Thus the system (3) becomes

$$\partial_t \widetilde{\mathbf{u}} + \sum_{\ell=1}^{2} \partial_{x_\ell} \widetilde{\mathbf{f}}_\ell(\widetilde{\mathbf{u}}) = \mathbf{0} \ \text{ in } \ G \times \mathbb{R}^+, \tag{19}$$

where $\widetilde{\mathbf{u}} = (\rho, \rho v_1, \rho v_2, \rho \widetilde{E})^T$, $\widetilde{\mathbf{f}}_\ell(\widetilde{\mathbf{u}}) = (\rho v_\ell,\ \rho v_\ell v_1 + \delta_1^\ell \widetilde{p},\ \rho v_\ell v_2 + \delta_2^\ell \widetilde{p},\ \rho \widetilde{H} v_\ell)^T$ and $\widetilde{p} = (\gamma - 1)\rho \left(\widetilde{E} - \frac{|\mathbf{v}|^2}{2}\right)$.

Smooth solutions of the system of the Euler equations exist in general only for short time and well-known phenomena like shock waves and contact discontinuities develop naturally. Hence we introduce the concept of weak solutions. A bounded set $\sigma \subset \mathbb{R}^2$ is said to be a control volume if Gauss' integral theorem is applicable to functions defined on σ. The mapping $\widetilde{\mathbf{u}}$ is called a weak solution of the system (19) if

$$\frac{d}{dt} \int_\sigma \widetilde{\mathbf{u}}\, d\mathbf{x} + \sum_{\ell=1}^{2} \int_{\partial\sigma} \widetilde{\mathbf{f}}_\ell(\widetilde{\mathbf{u}}) n_\ell \, ds = \mathbf{0} \tag{20}$$

is valid on every control volume $\sigma \subset G$ with outer unit normal vector $\mathbf{n} = (n_1, n_2)^T$.

Note that this formula can be derived from the system (19) by integrating over a control volume and applying Gauss' integral theorem. The solution class considered can be described by the function space $BV\left(\mathbb{R}_0^+; L^1 \cap L^\infty(\mathbb{R}^2; \mathbb{R}^4)\right)$, i.e. the mapping $t \mapsto \widetilde{\mathbf{u}}(\cdot, t)$ is of bounded variation and the image is an integrable function of the space variables which is bounded almost everywhere.

With respect to the numerical solution of equation (6) the space part G and the time part $\mathbb{R}^+$ have to be discretized. We are starting from an arbitrary conforming triangulation $\mathcal{T}_h$ which is usually called the primary mesh [21] and which consists of triangles $\mathcal{T}$. Furthermore, $\mathcal{N}_h$ denotes the index set of all nodes of the triangulation $\mathcal{T}_h$ and is subdivided by $\mathcal{N}_h = \mathcal{N}_{h,G} \cup \mathcal{N}_{h,\partial G}$, where $\mathcal{N}_{h,G}$ is associated with the inner points and $\mathcal{N}_{h,\partial G}$ includes the indices of the boundary points. Although a triangle itself can be used as a control volume, we consider boxes σ_i which are defined as the open set including the node $\mathbf{x}_i = (x_{i1}, x_{i2})^T$ (see Figure 1 (left)) and which are bounded by the straight lines l_{ij}^k, $k = 1, 2$, connecting the midpoint of the corresponding edge with the point $\mathbf{x}_s = (x_{s1}, x_{s2})^T$ (see Figure 1 (right)). Here $\mathbf{x}_s$ is defined by

$$\mathbf{x}_s = \sum_{m \in \{i,j,k\}} \alpha_m^s \mathbf{x}_m \ \text{ with } \ \alpha_m^s = \frac{1}{2\left(|l_i| + |l_j| + |l_k|\right)} \sum_{\substack{\overline{m} \in \{i,j,k\} \\ \overline{m} \neq m}} |l_{\overline{m}}|.$$

The union of these boxes σ_i, $i \in \mathcal{N}_h$, is called the secondary mesh.

Introducing the cell average

$$\widetilde{\mathbf{u}}_i(t) = \frac{1}{|\sigma_i|} \int_{\sigma_i} \widetilde{\mathbf{u}}(\mathbf{x}, t)\, d\mathbf{x},$$

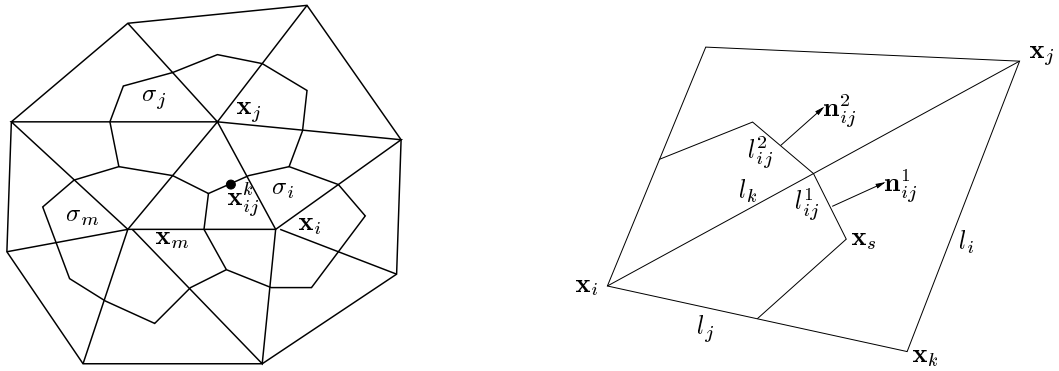

Figure 1: General form of a control volume of the triangulation $\mathcal{T}_h$ (left) and its boundary (right)

the integral form (20) with respect to an inner box σ_i can be written as

$$\frac{d}{dt}\widetilde{\mathbf{u}}_i(t) = -\frac{1}{|\sigma_i|}\sum_{j\in N(i)}\sum_{k=1}^{2}\int_{l_{ij}^k}\sum_{\ell=1}^{2}\widetilde{\mathbf{f}}_\ell(\widetilde{\mathbf{u}}(\mathbf{x},t))n_\ell\, ds, \tag{21}$$

where $N(i)$ denotes the index set of all neighbouring boxes of the control volume σ_i. Note that in the case of a boundary box σ_i, $i \in \mathcal{N}_{h,\partial G}$, the boundary conditions have to be considered additionally. Concerning the initial conditions the freestream values $(\rho_\infty, v_{1,\infty}, v_{2,\infty}, \widetilde{p}_\infty)^T$ are used to define the constant initial distribution via $\widetilde{\mathbf{u}}_0(\mathbf{x}) = \left(\rho_\infty, \rho_\infty v_{1,\infty}, \rho_\infty v_{2,\infty}, \frac{\widetilde{p}_\infty}{\gamma-1} + \frac{\rho_\infty |\mathbf{v}_\infty|^2}{2}\right)^T$.

Straightforward calculations prove the rotational invariance of the Euler equations such that (21) can be rewritten as

$$\frac{d}{dt}\widetilde{\mathbf{u}}_i(t) = -\frac{1}{|\sigma_i|}\sum_{j\in N(i)}\sum_{k=1}^{2}\int_{l_{ij}^k}\mathbf{T}^{-1}(\mathbf{n})\,\widetilde{\mathbf{f}}_1(\mathbf{T}(\mathbf{n})\,\widetilde{\mathbf{u}}(\mathbf{x},t))\, ds, \tag{22}$$

where the rotational matrix is given by

$$\mathbf{T}(\mathbf{n}) = \begin{pmatrix} 1 & 0 & 0 & 0 \\ 0 & n_1 & n_2 & 0 \\ 0 & -n_2 & n_1 & 0 \\ 0 & 0 & 0 & 1 \end{pmatrix}.$$

Note that in the case of a boundary box σ_i there exist two adjacent cells σ_j, $j \in \mathcal{N}_{h,\partial G}$, such that $\partial\sigma_i \cap \partial\sigma_j$ consists of one line segment l_{ij}^k only. In order to achieve a unique representation we interpret the lacking line segment as having the length zero. Obviously, the evaluation of the line integrals leads into trouble when $\widetilde{\mathbf{u}}$ is discontinuous across $\partial\sigma_i$. For the solution of these Riemann problems we introduce the concept of a numerical flux function which is often called a Riemann solver. During the past more than forty years a huge variety of numerical flux functions has been developed showing different advantages as well as failings [13, 68, 74, 17, 16, 57, 54, 30, 55]. Such schemes can be found in various well-written text books [70, 37, 23, 24, 12, 40].

In 1991 Liou and Steffen [41] proposed a new flux splitting scheme called AUSM (Advection Upstream Splitting Method) which successfully combines the accuracy of the flux difference splitting schemes with the simplicity of the flux vector splitting methods. Thus, the method is able to capture a stationary contact discontinuity without numerical diffusion and avoids the carbuncle phenomenon. Unfortunately it suffers from some difficulties like oscillations in the pressure distribution behind a moving shock. Three years later Liou and Wada [77] presented an improved AUSM which they called AUSMDV. This method combines the so-called AUSMD, AUSMV and Hänel's scheme including an additional numerical dissipation to remove the glitches at the sonic point within rarefaction waves. "D" and "V" means that the corresponding scheme is flux difference or flux vector splitting based, respectively. The method has desirable properties like no numerical dissipation on stationary and moving contact discontinuities as well as preserving enthalpy in steady flows, high resolution for shock waves and the scheme avoids pressure oscillations observed in the AUSM scheme. Furthermore, the resulting numerical flux function is continuously differentiable and can be extended to simulate chemically reacting [77, 18] as well as turbulent flow fields [48, 49] and was modified

for unsteady flow fields on moving grids [42]. With regard to these favourable properties we employ the AUSMDV scheme in the current numerical framework. Thus, we approximate the boundary integral from (22) by means of

$$\int_{l_{ij}^k} \mathbf{T}^{-1}\left(\mathbf{n}\right) \widetilde{\mathbf{f}}_1(\mathbf{T}\left(\mathbf{n}\right) \widetilde{\mathbf{u}}(\mathbf{x},t))\, ds = \left|l_{ij}^k\right| \mathbf{H}^{AUSMDV}\left(\widetilde{\mathbf{z}}_i, \widetilde{\mathbf{z}}_j; \mathbf{n}_{ij}^k\right). \tag{23}$$

Herein, $\widetilde{\mathbf{z}}_i$ and $\widetilde{\mathbf{z}}_j$ represent an approximation of the conserved variables at the left and right hand side of the midpoint $\mathbf{x}_{ij}^k$ corresponding to the line segment l_{ij}^k. Using the cell averages , i. e. $\widetilde{\mathbf{z}}_i = \widetilde{\mathbf{u}}_i$ and $\widetilde{\mathbf{z}}_j = \widetilde{\mathbf{u}}_j$, leads to a spatially first-order accurate scheme. The central approach for the construction of higher-order finite volume methods is based on the recovery of improved approximations $\widetilde{\mathbf{z}}_i$, $\widetilde{\mathbf{z}}_j$ from the given cell averages. A detailed introduction and mathematical analysis of different reconstruction technique is presented in [65]. Within this study we concentrate on the recovery based on linear polynomials. We employ two different approaches, namely a Total Variation Diminishing (TVD) like ansatz including the slope limiter of Barth and Jespersen [4] which is proposed in [44, 49] and a Weighted Essentially Non-Oscillatory (WENO) reconstruction technique following the work of Friedrich [9].

In the present study we distinguish three different types of boundary conditions: Fixed wall, inflow and outflow boundary. Therefore we subdivide the boundary of the triangulation into three parts $\partial\mathcal{T}_h = \partial\mathcal{T}_{h,w} \cup \partial\mathcal{T}_{h,in} \cup \partial\mathcal{T}_{h,out}$, where $\partial\mathcal{T}_{h,w}$, $\partial\mathcal{T}_{h,in}$, $\partial\mathcal{T}_{h,out}$ denote fixed wall, inflow and outflow parts, respectively. First, we require that no fluid particle can pass a solid wall. Thus we assume $v_{\mathbf{n}}(\mathbf{x},t) = \mathbf{v}(\mathbf{x},t)\cdot\mathbf{n}(\mathbf{x}) = 0$ for all $\mathbf{x} \in \partial\mathcal{T}_{h,w}$ and $t \in \mathbb{R}_0^+$. Consequently, the mass flux as well as the energy flux through this boundary vanish and we obtain

$$\int_{\partial\sigma_i \cap \partial\mathcal{T}_{h,w}} \mathbf{T}^{-1}\left(\mathbf{n}\right) \widetilde{\mathbf{f}}_1(\mathbf{T}\left(\mathbf{n}\right) \widetilde{\mathbf{u}}(\mathbf{x},t))\, ds = \sum_{l_{\sigma_i} \subset \partial\mathcal{T}_{h,w}} |l_{\sigma_i}| \begin{pmatrix} 0 \\ \widetilde{p}(\mathbf{x}_i^m,t)\cdot\mathbf{n}_{\sigma_i} \\ 0 \end{pmatrix}, \tag{24}$$

where $\mathbf{x}_i^m$ represents the midpoint of the line segment l_{σ_i} (see Figure 2). Note that the pressure $\widetilde{p}$ is defined by means of the constant or linear distribution $\widetilde{\mathbf{z}}_i$ and no evaluation of a numerical flux function is necessary. Furthermore, the fluxes through the inflow and outflow parts are approximated by

$$\int_{\partial\sigma_i \cap \partial\mathcal{T}_{h,in}} \mathbf{T}^{-1}\left(\mathbf{n}\right) \widetilde{\mathbf{f}}_1(\mathbf{T}\left(\mathbf{n}\right) \widetilde{\mathbf{u}}(\mathbf{x},t))\, ds = \sum_{l_{\sigma_i} \subset \partial\mathcal{T}_{h,in}} |l_{\sigma_i}| \mathbf{H}^{AUSMDV}\left(\widetilde{\mathbf{z}}_i, \widetilde{\mathbf{z}}_\infty; \mathbf{n}_{\sigma_i}\right) \tag{25}$$

and

$$\int_{\partial\sigma_i \cap \partial\mathcal{T}_{h,out}} \mathbf{T}^{-1}\left(\mathbf{n}\right) \widetilde{\mathbf{f}}_1(\mathbf{T}\left(\mathbf{n}\right) \widetilde{\mathbf{u}}(\mathbf{x},t))\, ds = \sum_{l_{\sigma_i} \subset \partial\mathcal{T}_{h,out}} |l_{\sigma_i}| \mathbf{H}^{AUSMDV}\left(\widetilde{\mathbf{z}}_i, \widetilde{\mathbf{z}}_i; \mathbf{n}_{\sigma_i}\right), \tag{26}$$

respectively. It is mentionable that the consistency of the numerical flux function yields $\mathbf{H}^{AUSMDV}\left(\widetilde{\mathbf{z}}_i, \widetilde{\mathbf{z}}_i; \mathbf{n}_{\sigma_i}\right) = \mathbf{T}^{-1}\left(\mathbf{n}_{\sigma_i}\right) \widetilde{\mathbf{f}}_1(\mathbf{T}\left(\mathbf{n}_{\sigma_i}\right) \widetilde{\mathbf{z}}_i)$.

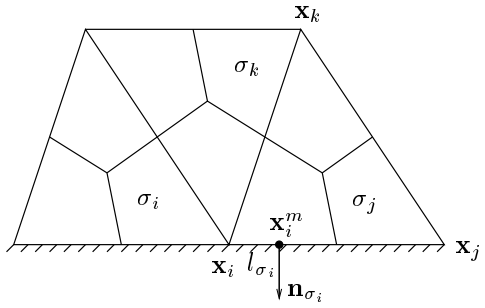

Figure 2: Boundary control volume

With respect to the asymptotic analysis of the numerical method it is necessary to explicitly point out the numerical flux function employed. First, we introduce the AUSMD-type scheme. Here the numerical flux is defined by

$$\mathbf{H}^{AUSMD}(\widetilde{\mathbf{z}}_L, \widetilde{\mathbf{z}}_R; \mathbf{n}) = \frac{1}{2}\left((\rho v_{\mathbf{n}})_{1/2}(\Phi_L + \Phi_R) + |(\rho v_{\mathbf{n}})_{1/2}|(\Phi_L - \Phi_R)\right) + \Psi_{1/2}, \tag{27}$$

where $\Phi = \left(1, v_{\mathbf{n}}, v_{\mathbf{t}}, \widetilde{H}\right)^T$, $\Psi_{1/2} = \left(0, \widetilde{p}_{1/2}, 0, 0\right)^T$ and the indices $\mathbf{n}$ and $\mathbf{t}$ denote the velocity components perpendicular and parallel to the edge, respectively. In order to capture steady as well as moving contact discontinuities,

we define the coefficients $\alpha_L = \frac{2(\widetilde{p}/\rho)_L}{(\widetilde{p}/\rho)_L+(\widetilde{p}/\rho)_R}$, $\alpha_R = \frac{2(\widetilde{p}/\rho)_R}{(\widetilde{p}/\rho)_L+(\widetilde{p}/\rho)_R}$ and $\widetilde{c}_m = \max\{\widetilde{c}_L, \widetilde{c}_R\}$. If $\widetilde{\mathrm{Ma}}_{\mathbf{n},L/R} := \frac{v_{\mathbf{n},L/R}}{\widetilde{c}_m}$, then the pressure flux is given by

$$\widetilde{p}_{1/2} = \widetilde{p}_L^+ + \widetilde{p}_R^- \tag{28}$$

where

$$\widetilde{p}_{L/R}^{\pm} = \begin{cases} \frac{1}{4}\,\widetilde{p}_{L/R}\,\left(\widetilde{\mathrm{Ma}}_{\mathbf{n},L/R} \pm 1\right)^2\left(2 \mp \widetilde{\mathrm{Ma}}_{\mathbf{n},L/R}\right), & \text{if } \left|\widetilde{\mathrm{Ma}}_{\mathbf{n},L/R}\right| \le 1 \\ \frac{1}{2}\,\widetilde{p}_{L/R}\,\frac{v_{\mathbf{n},L/R} \pm |v_{\mathbf{n},L/R}|}{v_{\mathbf{n},L/R}}, & \text{otherwise.} \end{cases} \tag{29}$$

The velocity splitting reads

$$v_{\mathbf{n},L/R}^{\pm} = \begin{cases} \alpha_{L/R}\left\{\pm\frac{\left(v_{\mathbf{n},L/R} \pm \widetilde{c}_m\right)^2}{4\,\widetilde{c}_m} - \frac{v_{\mathbf{n},L/R} \pm |v_{\mathbf{n},L/R}|}{2}\right\} + \frac{v_{\mathbf{n},L/R} \pm |v_{\mathbf{n},L/R}|}{2}, & \text{if } \left|\widetilde{\mathrm{Ma}}_{\mathbf{n},L/R}\right| \le 1 \\ \frac{v_{\mathbf{n},L/R} \pm |v_{\mathbf{n},L/R}|}{2}, & \text{otherwise.} \end{cases} \tag{30}$$

Thus, the mass flux splitting $(\rho v_{\mathbf{n}})_{1/2} = v_{\mathbf{n},L}^+\,\rho_L + v_{\mathbf{n},R}^-\,\rho_R$ is well-defined. Secondly, we consider the AUSMV-type scheme. This scheme differs from the AUSMD-type scheme only in the first momentum flux, which is given by

$$\mathbf{H}_{m_1}^{AUSMV}(\widetilde{\mathbf{z}}_L, \widetilde{\mathbf{z}}_R; \mathbf{n}) = v_{\mathbf{n},L}^+\,(\rho v_{\mathbf{n}})_L + v_{\mathbf{n},R}^-\,(\rho v_{\mathbf{n}})_R + \widetilde{p}_{1/2}.$$

Liou and Wada observed in numerical investigations, that the AUSMV has a higher shock capturing capability than the AUSMD but produces oscillations in the velocity field behind moving contact discontinuities [77]. According to these properties a mixed numerical flux in the form

$$\mathbf{H}^{AUSMD+V}(\widetilde{\mathbf{z}}_L, \widetilde{\mathbf{z}}_R; \mathbf{n}) = \left(\frac{1}{2} + s\right)\mathbf{H}^{AUSMV}(\widetilde{\mathbf{z}}_L, \widetilde{\mathbf{z}}_R; \mathbf{n}) + \left(\frac{1}{2} - s\right)\mathbf{H}^{AUSMD}(\widetilde{\mathbf{z}}_L, \widetilde{\mathbf{z}}_R; \mathbf{n}) \tag{31}$$

is used, where $s := \frac{1}{2}\min\left(1, K\frac{|\widetilde{p}_R - \widetilde{p}_L|}{\min\{\widetilde{p}_R, \widetilde{p}_L\}}\right)$. Analogously to [77] a parameter $K = 10$ is employed. Two problems of this scheme have to be overcome. First, there are glitches at an expansive sonic point. In this case an additional numerical dissipation is used. We detect the sonic point within a rarefaction wave with the help of $A := ((v_{\mathbf{n},L} - \widetilde{c}_L) < 0)\,\&\,((v_{\mathbf{n},R} - \widetilde{c}_R) > 0)$ and $B := ((v_{\mathbf{n},L} + \widetilde{c}_L) < 0)\,\&\,((v_{\mathbf{n},R} + \widetilde{c}_R) > 0)$ and we define the dissipation function in the form

$$\mathbf{H}^{DIFF}(\widetilde{\mathbf{z}}_L, \widetilde{\mathbf{z}}_R; \mathbf{n}) = \begin{cases} C\left[(v_{\mathbf{n},L} - \widetilde{c}_L) - (v_{\mathbf{n},R} - \widetilde{c}_R)\right]\left[(\rho\Phi)_L - (\rho\Phi)_R\right], & \text{if } A\,\&\,\neg B \\ C\left[(v_{\mathbf{n},L} + \widetilde{c}_L) - (v_{\mathbf{n},R} + \widetilde{c}_R)\right]\left[(\rho\Phi)_L - (\rho\Phi)_R\right], & \text{if } \neg A\,\&\,B \\ \mathbf{0}, & \text{otherwise} \end{cases} \tag{32}$$

with the constant $C = 0.125$. Second, we are faced with the so called carbuncle phenomenon. This phenomenon represents a numerical instability which probably comes from the interaction of unphysical values of the flow variables inside of discrete shock waves calculated by a one-dimensional scheme in a multi-dimensional flow. Analogously to the numerical flux function of Roe [57] and Osher [54], the scheme (31) described above suffers from this oscillation problem. Hence a more dissipative scheme is required in this case to stabilize the shock wave. Liou and Wada employed Hänel's scheme [16] where the numerical flux is given by

$$\mathbf{H}^{Hänel}(\widetilde{\mathbf{z}}_L, \widetilde{\mathbf{z}}_R; \mathbf{n}) := v_{\mathbf{n},L}^+\rho_L\Phi_L + v_{\mathbf{n},R}^-\rho_R\Phi_R + \Psi_{1/2}. \tag{33}$$

Here the velocity splitting and the interface pressure are defined by equation (30) and equations (28), (29) with the modification $\alpha_L = \alpha_R = 1$ and $\widetilde{c}_m = \widetilde{c}_L$ or $\widetilde{c}_R$, respectively. For the localization of the shock wave we use

$$S_i := \begin{cases} 1, & \text{if } \exists\, j \in N(i) \quad \text{with } (v_{\mathbf{n},i} - \widetilde{c}_i) > 0\ \&\ (v_{\mathbf{n},j} - \widetilde{c}_j) < 0 \text{ or } (v_{\mathbf{n},i} + \widetilde{c}_i) > 0\ \&\ (v_{\mathbf{n},j} + \widetilde{c}_j) < 0 \\ 0, & \text{otherwise.} \end{cases} \tag{34}$$

With application of (31) we finally obtain our numerical flux function in the form

$$\begin{aligned} &\mathbf{H}^{AUSMDV}(\widetilde{\mathbf{z}}_L, \widetilde{\mathbf{z}}_R; \mathbf{n}) \\ &= \mathbf{T}^{-1}(\mathbf{n})\Big\{\delta_2^{(S_L+S_R)}\mathbf{H}^{Hänel}(\widetilde{\mathbf{z}}_L, \widetilde{\mathbf{z}}_R; \mathbf{n}) \\ &\qquad + \left(1 - \delta_2^{(S_L+S_R)}\right)\left(\mathbf{H}^{AUSMD+V}(\widetilde{\mathbf{z}}_L, \widetilde{\mathbf{z}}_R; \mathbf{n}) + \mathbf{H}^{DIFF}(\widetilde{\mathbf{z}}_L, \widetilde{\mathbf{z}}_R; \mathbf{n})\right)\Big\}. \end{aligned} \tag{35}$$

The equation (22) in conjunction with (23) exhibits that now the conservation laws have been transformed into a system of ordinary differential equations. Concerning the time discretization we take advantage of the fact that we restrict ourself to the consideration of steady flow fields. Thus we utilize very simple first order time stepping techniques, namely the so called forward and backward Euler differences. Hence the complete numerical method reads as

$$\mathbf{u}_i^{n+1} = \mathbf{u}_i^n - \frac{\Delta t}{|\sigma_i|} \sum_{j \in N(i)} \sum_{k=1}^{2} \left| l_{ij}^k \right| \mathbf{H}^{AUSMDV} \left(\tilde{\mathbf{z}}_i^m, \tilde{\mathbf{z}}_j^m; \mathbf{n}_{ij}^k \right), \tag{36}$$

where $m \in \{n, n+1\}$, $\mathbf{u}_i^n = \mathbf{u}_i(t^n)$, and $t^{n+1} = t^n + \Delta t$. In the case of an implicit approach, i.e. $m = n+1$, a linearization of the numerical flux function is performed which leads to a linear system of equations including a large, sparse and usually unsymmetric matrix. The performance of an implicit method decisively depends on the properties of the incorporated solver for the linear system of equations. Based on a systematic investigation and comparison of Krylov subspace methods [44] we decided to apply the BiCGSTAB algorithm developed by van der Vorst [73] but in a preconditioned formulation, see [51]. For a comprehensive derivation and analysis of different Krylov subspace methods we refer to [3, 58, 15, 46] and the literature therein.

3.1. Numerical results for compressible flows

In advance to the investigation of the numerical method with respect to low Mach number fluid flow we have to ensure the validity of the described scheme in the trans-, super- and hypersonic regime. Therefore we have chosen several well-known test cases from computational fluid dynamics which are consolidated in Table 1.

Configuration	$\widetilde{\mathrm{Ma}}_\infty = \frac{\lvert \mathbf{v}_\infty \rvert}{\tilde{c}_\infty}$	Angle of attack	Recovery technique	References
SKF 1.1 airfoil	0.65	3°	WENO	[67]
RAE2822 airfoil	0.75	3°	WENO	[56]
NACA0012 airfoil	0.8	1.25°	WENO	[36]
Combustion chamber	2.0	0°	TVD	[78]
Cylinder	10.0	0°	WENO	

Table 1: Trans-, super-, and hypersonic inviscid test cases

The first test case shows the transsonic flow about the SKF 1.1 two element airfoil [67] at $\widetilde{\mathrm{Ma}}_\infty = 0.65$ and an angle of attack $\alpha = 3°$ (see Figure 3). In order to validate our numerical method by the experimental data, it must be corrected for wall interferences [66]. To overcome the high value of the lift coefficient, we use $\alpha = -0.25°$ for our scheme. From the comparison (Figure 4) between the computed and the experimental C_p-values, it is obvious that our numerical data gives a good approximation of the real physical phenomenon.

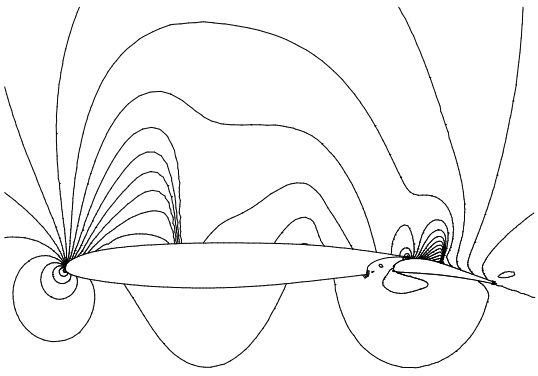

Figure 3: Isolines of the density distribution in the vicinity of the airfoil

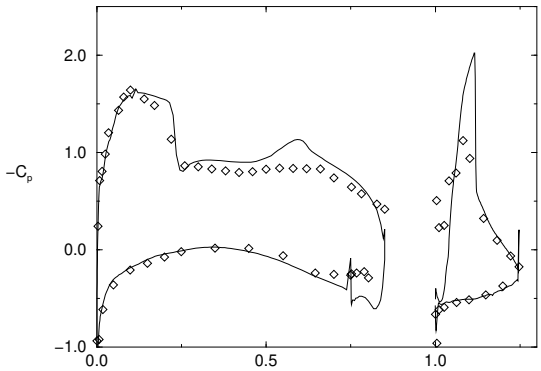

Figure 4: Comparison of the C_p-distribution, – Finite-volume scheme, ⋄ Reference data [67]

The second transsonic test case represents a steady state flow past the RAE2822 airfoil at a freestream Mach number $\widetilde{\mathrm{Ma}}_\infty = 0.75$ and $\alpha = 3°$. The density distribution obtained is shown in Figure 5. From Figure 6 we can learn about the good correspondence between the computed C_p-distribution and the results presented during a GAMM workshop [56].

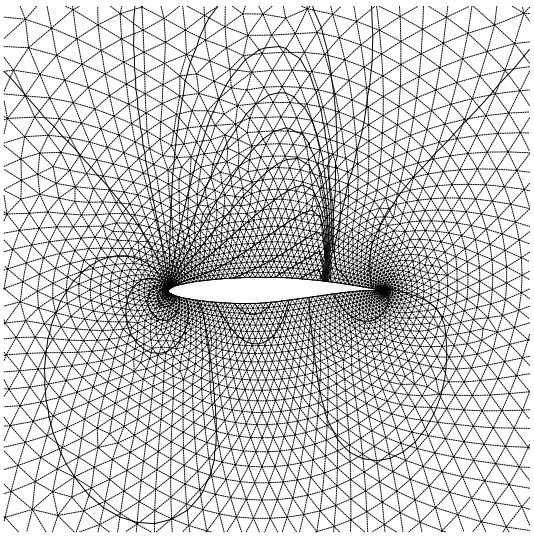

Figure 5: Isolines of the density distribution in the vicinity of the airfoil

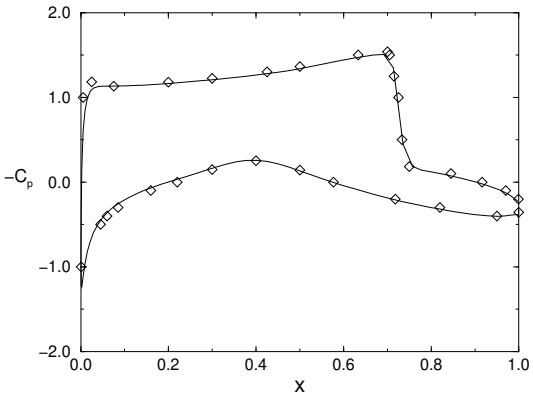

Figure 6: Comparison of the C_p-distribution, – Finite volume scheme, $\diamond$ Reference data [56]

Concerning the transsonic regime we finally regard the flow about the NACA0012 airfoil at $\widetilde{\mathrm{Ma}}_\infty = 0.8$ and $\alpha = 1.25°$. The isolines of the density distributions are depicted in Figure 7 and Figure 8 shows a comparison of our computed C_p-distribution with the results obtained by Thomas [69] on a structured grid with a dicretization method similar to Jameson's [30].

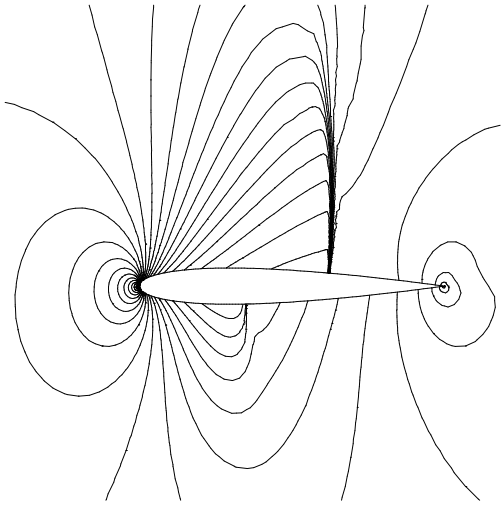

Figure 7: Isolines of the density distribution in the vicinity of the airfoil

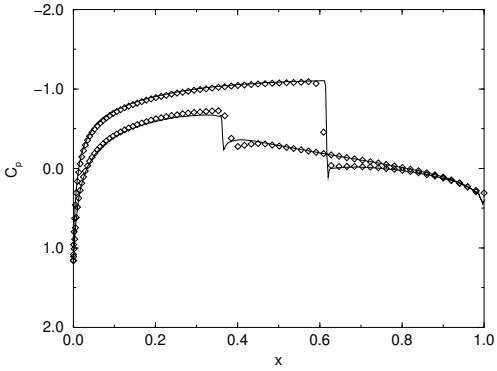

Figure 8: C_p distribution, – Finite volume scheme, $\diamond$ Reference data [69]

In order to indicate the accuracy and performance of the presented finite volume scheme in the context of supersonic flow fields we consider the remaining two test cases. The first test case is concerned with the simulation of a supersonic steady state flow through a combustion chamber. The flow field features a complicated pattern of shock and rarefaction waves as well as contact discontinuities. As one can see from Figure 9 all these features mentioned are resolved sharply.

We finish the evaluation of the described numerical scheme by means of a hypersonic flow past a cylinder at

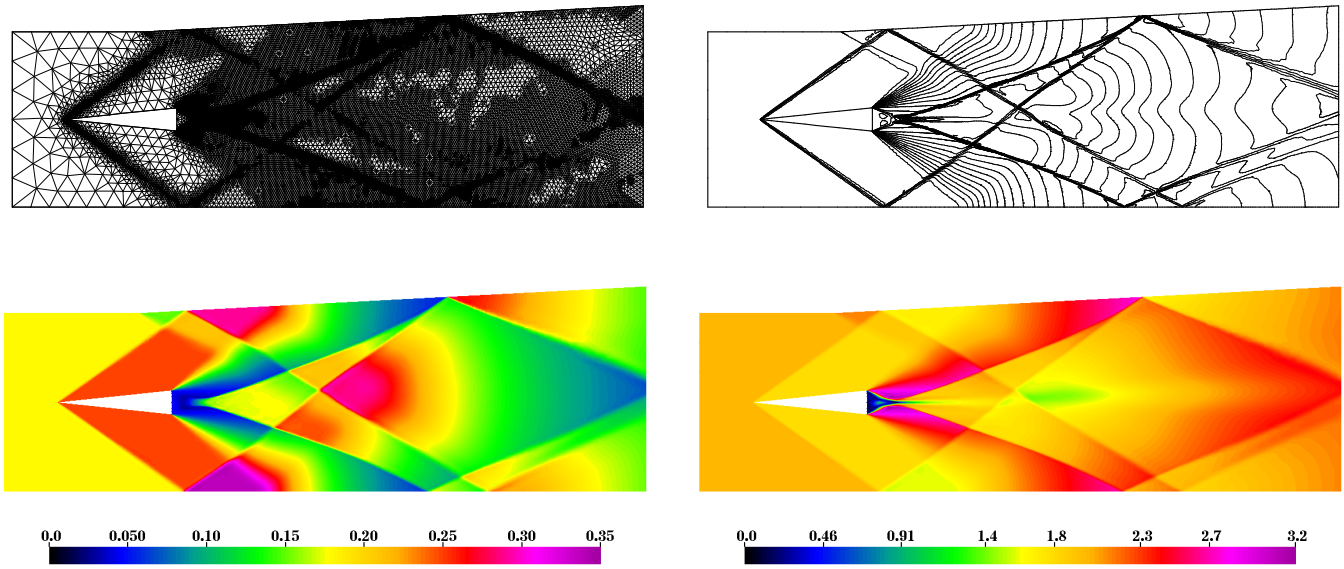

Figure 9: Triangulation of the combustion chamber (top, left), isolines of the density distribution (top, right), pressure distribution (bottom, left), local Mach number distribution $\widetilde{\mathrm{Ma}} = |\mathbf{v}|/\tilde{c}$ (bottom, right)

$\widetilde{\mathrm{Ma}}_\infty = 10.0$. In Figure 10 we present the computed pressure and density distribution. For the validation of our results, we also show the Mach number distribution along the stagnation point line, see Figure 11. The shock location is in excellent accordance with the analytic value (represented as the dashed line in Figure 11) obtained from [1].

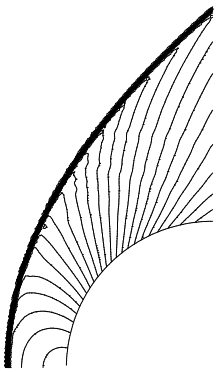

Figure 10: Isolines of pressure

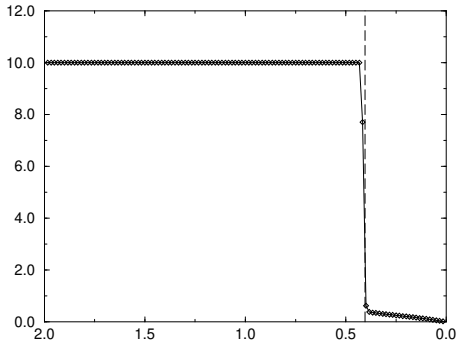

Figure 11: Mach number distribution along the stagnation point line

The union of all these test cases emphasize the validity, stability and high resolution properties of the finite volume approximation in the field of trans-, super-, and hypersonic inviscid fluid flow.

3.2. Asymptotic analysis

The objective of this section is the theoretical investigation of the finite volume scheme in the low Mach number limit. For the sake of simplicity we consider the first order accurate approximation, i.e. $\widetilde{\mathbf{z}}_i = \widetilde{\mathbf{u}}_i$, $\widetilde{\mathbf{z}}_j = \widetilde{\mathbf{u}}_j$, in an explicit formulation.

The transition between subsonic and supersonic parts of the flow field represents a feature of transsonic fluid flow and does not occur in the low Mach number regime. As a consequence we obtain from (34) the statement $S_i = 0$ for

all $i \in \mathcal{N}_h$, and thus the influence of the dissipative numerical flux function $\mathbf{H}^{Hänel}$ vanishes within the AUSMDV scheme, see equation (35). Furthermore, the Boolean numbers A, B used for the definition of $\mathbf{H}^{DIFF}$ are always zero, so that we can disregard the impact of this function in the low Mach number regime and the AUSMDV scheme (35) finally takes the form

$$\mathbf{H}^{AUSMDV}(\widetilde{\mathbf{z}}_L, \widetilde{\mathbf{z}}_R; \mathbf{n}) = \mathbf{T}^{-1}(\mathbf{n})\mathbf{H}^{AUSMD+V}(\widetilde{\mathbf{z}}_L, \widetilde{\mathbf{z}}_R; \mathbf{n}). \tag{37}$$

Although the numerical flux function is significantly easier to investigate in the absence of sonic points, several quiet different ingredients still remain within the AUSMDV scheme. Due to that fact we proceed as follows: First we introduce the abbreviation

$$\Delta_{ij}\varphi = \varphi_i - \varphi_j,$$

second we successively analyze some important parts of the flux function to achieve statements concerning their proportion and third we merge these facts and prove statements concerning the behaviour of the whole finite volume method in the low Mach number limit.

Using a simple retransformation of the auxiliary variables defined by (18) into the corresponding physical quantities yields the following order relation for $\widetilde{\mathrm{Ma}}_{\mathbf{n},i/j}$ in the form

$$\widetilde{\mathrm{Ma}}_{\mathbf{n},i/j} = \frac{|v_{\mathbf{n},i/j}|}{\widetilde{c}_m} = \mathrm{M}\underbrace{\frac{|v_{\mathbf{n},i/j}|}{c_m}}_{=\mathrm{Ma}_{\mathbf{n},i/j}=O(1)} = O(\mathrm{M}), \quad \mathrm{M} \to 0. \tag{38}$$

Furthermore the auxiliary pressure variable $\widetilde{p}^{\pm}_{i/j}$ (see (29)) satisfies

$$\widetilde{p}^{\pm}_{i/j} = \frac{1}{4}p_{i/j}\left(\frac{2}{\mathrm{M}^2} \pm \frac{3\mathrm{Ma}_{\mathbf{n},i/j}}{\mathrm{M}} \mp \mathrm{M}\mathrm{Ma}^3_{\mathbf{n},i/j}\right) \tag{39}$$

and the velocity component in normal direction (30) can be written as

$$v^{\pm}_{\mathbf{n},i/j} = \pm\frac{1}{\mathrm{M}}\frac{\alpha_{i/j}c_m}{4} + \left(1-\alpha_{i/j}\right)\frac{v_{\mathbf{n},i/j} \pm |v_{\mathbf{n},i/j}|}{2} + \frac{\alpha_{i/j}v_{\mathbf{n},i/j}}{2} \pm \mathrm{M}\frac{\alpha_{i/j}v_{\mathbf{n},i/j}}{c_m} \tag{40}$$

by means of the coefficients $\alpha_{i/j} = \frac{2(p/\rho)_{i/j}}{(p/\rho)_i + (p/\rho)_j}$. The equation (40) yields a first hint concerning a potential failure of the scheme in the low Mach number regime since it is currently obvious that the numerical velocity component in normal direction and its physical counterpart are of different orders with respect to a vanishing Mach number. Composing the statements outlined above, the mass flux provided by the AUSMDV scheme takes the form

$$\begin{aligned}\mathbf{H}^{AUSMDV}_{\rho}(\widetilde{\mathbf{u}}_i, \widetilde{\mathbf{u}}_j; \mathbf{n}) &= \frac{1}{2\mathrm{M}}\frac{c_m}{(p/\rho)_i + (p/\rho)_j}\Delta_{ij}p + (1-\alpha_i)\rho_i\frac{v_{\mathbf{n},i} + |v_{\mathbf{n},i}|}{2} \\ &\quad + (1-\alpha_j)\rho_j\frac{v_{\mathbf{n},j} - |v_{\mathbf{n},j}|}{2} + \frac{\Delta_{ij}(pv_{\mathbf{n}})}{(p/\rho)_i + (p/\rho)_j} + O(\mathrm{M}), \quad \mathrm{M} \to 0.\end{aligned} \tag{41}$$

In contrast to the continuity equation the momentum fluxes of the AUSMD and AUSMV method are different and have to be considered separately. In the case of the AUSMD scheme we state

$$\begin{aligned}&\frac{1}{2}\left\{(\rho v_{\mathbf{n}})_{1/2}\left(v_{\mathbf{n},i} + v_{\mathbf{n},j}\right) + |\,(\rho v_{\mathbf{n}})_{1/2}\,|\left(v_{\mathbf{n},i} - v_{\mathbf{n},j}\right)\right\} \\ &\quad = \frac{1}{4\mathrm{M}}\frac{c_m}{(p/\rho)_i + (p/\rho)_j}\Big((v_{\mathbf{n},i} + v_{\mathbf{n},j})\Delta_{ij}p + \Delta_{ij}v_{\mathbf{n}}|\Delta_{ij}p|\Big) + O(1), \quad \mathrm{M} \to 0,\end{aligned} \tag{42}$$

whereas the AUSMV method includes the term

$$v^{+}_{\mathbf{n},i}(\rho v_{\mathbf{n}})_i + v^{-}_{\mathbf{n},j}(\rho v_{\mathbf{n}})_j = \frac{1}{2\mathrm{M}}\frac{c_m}{(p/\rho)_i + (p/\rho)_j}\Delta_{ij}\left(pv_{\mathbf{n}}\right) + O(1), \quad \mathrm{M} \to 0. \tag{43}$$

It is easily seen that the weight factor s fulfills $s = O(1)$, $\mathrm{M} \to 0$, so that (42) and (43) lead to the expression for the components of the numerical momentum flux in x_1-direction in the form

$$\begin{aligned}
&\mathbf{H}_{m_1}^{AUSMDV}(\widetilde{\mathbf{u}}_i, \widetilde{\mathbf{u}}_j; \mathbf{n}) \\
&= \frac{1}{\mathrm{M}^2}\frac{p_i + p_j}{2} n_1 + \frac{1}{\mathrm{M}}\frac{3}{4c_m}\Delta_{ij}\left(p v_{\mathbf{n}}\right) n_1 \\
&\quad + \frac{1}{4\mathrm{M}}\frac{c_m}{(p/\rho)_i + (p/\rho)_j}\left(\frac{\Delta_{ij}p}{2}(v_{\mathbf{n},i} + v_{\mathbf{n},j}) n_1 + \frac{|\Delta_{ij}p|}{2}(v_{\mathbf{n},i} - v_{\mathbf{n},j}) n_1 + \Delta_{ij}\left(p v_{\mathbf{n}}\right) n_1 \right. \\
&\qquad\qquad \left. - \frac{\Delta_{ij}p}{2}(v_{\mathbf{t},i} + v_{\mathbf{t},j}) n_2 - \frac{|\Delta_{ij}p|}{2}(v_{\mathbf{t},i} - v_{\mathbf{t},j}) n_2 \right) \\
&\quad + \frac{s}{4\mathrm{M}}\frac{c_m}{(p/\rho)_i + (p/\rho)_j}\left(\Delta_{ij}p(v_{\mathbf{n},i} + v_{\mathbf{n},j}) n_2 + |\Delta_{ij}p|(v_{\mathbf{n},i} - v_{\mathbf{n},j}) n_2 + 2\Delta_{ij}\left(p v_{\mathbf{n}}\right) n_2 \right) \\
&\quad + O(1), \quad \mathrm{M} \to 0.
\end{aligned} \tag{44}$$

Analogously, we can rewrite the numerical energy flux of the finite volume approximation as

$$\mathbf{H}_{(\rho\widetilde{E})}^{AUSMDV}(\widetilde{\mathbf{u}}_i, \widetilde{\mathbf{u}}_j; \mathbf{n}) = \frac{1}{4\mathrm{M}^3}\frac{c_m}{(p/\rho)_i + (p/\rho)_j}\Big(\Delta_{ij}p(H_i + H_j) + |\Delta_{ij}p|(H_i - H_j)\Big) + O\left(\frac{1}{\mathrm{M}^2}\right), \quad \mathrm{M} \to 0. \tag{45}$$

In accordance to the continuous asymptotic analysis we introduce a discrete asymptotic expansion originally proposed by Viozat and Guillard [14]. Similar to (6) we assume that each physical cell average $\varphi_i \in \{\rho_i, v_{1,i}, v_{2,i}, p_i, E_i\}$ with respect to the box σ_i, $i \in \mathcal{N}_h$, can be expressed in the form of an asymptotic single scale expansion

$$\varphi_i(t; \mathrm{M}) = \sum_{m=0}^{j} \mathrm{M}^m \varphi_i^{(m)}(t) + o\left(\mathrm{M}^j\right), \quad \mathrm{M} \to 0, \quad j = 0, 1, 2. \tag{46}$$

Introducing the expansion (46) into the finite volume method leads to the following version of the semidiscrete mass and energy equations with respect to an inner control volume σ_i, $i \in \mathcal{N}_{h,G}$:

$$\frac{d}{dt}\rho_i = -\frac{1}{\mathrm{M}}\frac{1}{|\sigma_i|}\sum_{j \in N(i)}\sum_{k=1}^{2}\frac{\eta_{ij}}{2}\Delta_{ij}p\,\left|l_{ij}^k\right| + O(1), \quad \mathrm{M} \to 0, \tag{47}$$

$$\frac{d}{dt}(\rho E)_i = -\frac{1}{\mathrm{M}}\frac{1}{|\sigma_i|}\sum_{j \in N(i)}\sum_{k=1}^{2}\frac{\eta_{ij}}{4}\Big(\Delta_{ij}p(H_i + H_j) + |\Delta_{ij}p|\,(H_i - H_j)\Big)\left|l_{ij}^k\right| + O(1), \quad \mathrm{M} \to 0, \tag{48}$$

whereby $\eta_{ij} = \frac{c_m}{(p/\rho)_i + (p/\rho)_j}$. Identifying terms multiplied by the same power of M enables the exploration of the discrete asymptotic leading as well as of the first order pressure term in the low Mach number regime. First we obtain from (47) and (48) the so called perturbation equations

$$0 = \sum_{j \in N(i)}\sum_{k=1}^{2}\frac{\eta_{ij}^{(0)}}{2}\Delta_{ij}p^{(0)}\,\left|l_{ij}^k\right| \tag{49}$$

and

$$0 = \sum_{j \in N(i)}\sum_{k=1}^{2}\frac{\eta_{ij}^{(0)}}{4}\left(\Delta_{ij}p^{(0)}(H_i^{(0)} + H_j^{(0)}) + \left|\Delta_{ij}p^{(0)}\right|(H_i^{(0)} - H_j^{(0)})\right)\left|l_{ij}^k\right|, \tag{50}$$

respectively. Taking into account $\eta_{ij}^{(0)} = \frac{c_m^{(0)}}{(p^{(0)}/\rho^{(0)})_i + (p^{(0)}/\rho^{(0)})_j} > 0$, we can directly conclude from (49) that the minimum as well as the maximum leading order pressure value has to be located within a boundary control volume σ_k, $k \in \mathcal{N}_{h,\partial G}$. In order to obtain also statements with respect to the pressure cell average p_i within boundary control volumes, we have to explore the numerical boundary fluxes (24), (25) and (26) additionally. The boundary

condition for an impermeable wall prohibits mass flux and energy flux through such boundary parts. Consequently, both equations (49) and (50) are unaffected by the flux through line segments $l_{\sigma_i} \subset \partial\mathcal{T}_{h,w}$. Let us now focus our attention to the inflow boundaries. Utilizing $\widetilde{\mathbf{z}}_j = \widetilde{\mathbf{z}}_i$ we obtain $\Delta_{ij}p^{(0)} = \Delta_{ii}p^{(0)} = 0$, and as a consequence

$$\mathbf{H}_\rho(\widetilde{\mathbf{z}}_i, \widetilde{\mathbf{z}}_j, \mathbf{n}) = O(1), \quad \mathrm{M} \to 0,$$

holds which implies that there will not appear an additional term within equation (49) with respect to the approximation of inflow parts. Exclusively, the outflow boundary affects the perturbation equation (49). Thus we can extend the validity of equation (49) from $i \in \mathcal{N}_{h,G}$ to $i \in \mathcal{N}_h$ by writing

$$0 = \vartheta_i \frac{\eta_{i\infty}^{(0)}}{2} \Delta_{i\infty} p^{(0)} \left| l_{\sigma_i} \right| + \sum_{j \in N(i)} \sum_{k=1}^{2} \frac{\eta_{ij}^{(0)}}{2} \Delta_{ij} p^{(0)} \left| l_{ij}^k \right|, \tag{51}$$

where ϑ_i represents the number of line segments $l_{\sigma_i} \subset \partial\sigma_i$ satisfying $l_{\sigma_i} \subset \partial\mathcal{T}_{h,out}$. As mentioned above there always exists an index $i \in \mathcal{N}_{h,\partial G}$ such that $p_i^{(0)} = \max_{k \in \mathcal{N}_h} p_k^{(0)}$. Introducing this property into (51) yields

$$\vartheta_i \underbrace{\frac{\eta_{i\infty}^{(0)}}{2}}_{>0} \Delta_{i\infty} p^{(0)} \underbrace{\left| l_{\sigma_i} \right|}_{>0} = - \sum_{j \in N(i)} \sum_{k=1}^{2} \underbrace{\frac{\eta_{ij}^{(0)}}{2}}_{>0} \underbrace{\Delta_{ij} p^{(0)}}_{\geq 0} \underbrace{\left| l_{ij}^k \right|}_{>0} \leq 0. \tag{52}$$

Obviously, we directly obtain $p_i^{(0)} = p_j^{(0)}$ for all $j \in N(i)$ if $\vartheta_i = 0$. On the other hand, we can conclude $p_i^{(0)} - p_\infty^{(0)} \leq 0$ if $\vartheta_i > 0$ which immediately proves the statement

$$p_\infty^{(0)} = \max_{k \in \mathcal{N}_h} p_k^{(0)}$$

with regard to the initial conditions. Similarly, we obtain $p_\infty^{(0)} = \min_{k \in \mathcal{N}_h} p_k^{(0)}$. Assembling both results shows that the discrete leading order pressure term is spatially constant in accordance to the behaviour in the continuous case.

Note that we can likewise prove the same property by means of the energy equation instead of the mass conservation law.

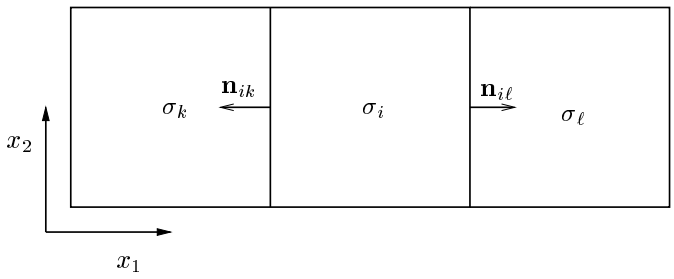

Figure 12: Notation used in the structured mesh

To derive statements concerning the discrete first order pressure distribution $p_i^{(1)}$, $i \in \mathcal{N}_h$, we consider a structured mesh depicted in Figure 12. We will now present an evidence of variations within the first order pressure field which are in contradiction to the results of the continuous asymptotic analysis. Therefore we determine the following assumptions:

$$i \in \mathcal{N}_{h,G}, \tag{53}$$

$$\rho_i^{(0)} = \rho_j^{(0)} \quad \text{for all} \quad j \in N(i) \tag{54}$$

and

$$v_{k,1}^{(0)} - v_{i,1}^{(0)} = v_{i,1}^{(0)} - v_{\ell,1}^{(0)} \neq 0. \tag{55}$$

Due to the fact that the leading order pressure term is spatially constant we obtain from the assumption (54) the expression

$$c_m^{(0)} = \max\{c_i^{(0)}, c_j^{(0)}\} = c_i^{(0)} =: c^{(0)}$$

for all $j \in N(i)$. Furthermore, the order relation with respect to the weight factor s can be aggravated to

$$s = \frac{1}{2}\min\left(1, K\frac{|p_j - p_i|}{\min\{p_j, p_i\}}\right) = \frac{1}{2}\min\left(1, \mathrm{M}K\frac{\left|p_j^{(1)} - p_i^{(1)}\right|}{\min\{p_j, p_i\}}\right) = O(\mathrm{M}), \quad \mathrm{M} \to 0.$$

Thus introducing the asymptotic expansion into the numerical momentum flux (44) and taking account of $\Delta_{ij}p^{(0)} = 0$ yields

$$\mathbf{H}_{m_1}^{AUSMDV}(\widetilde{\mathbf{z}}_i, \widetilde{\mathbf{z}}_j, \mathbf{n}) = \frac{1}{\mathrm{M}^2}p^{(0)}n_1 + \frac{1}{\mathrm{M}}\left(\frac{p_i^{(1)} + p_j^{(1)}}{2} + \left(\frac{3p^{(0)}}{4c^{(0)}} + \eta_{ij}^{(0)}p^{(0)}\right)\Delta_{ij}v_{\mathbf{n}}^{(0)}\right)n_1 + O(1), \quad \mathrm{M} \to 0,$$

where $p^{(0)} = p_i^{(0)} = p_j^{(0)}$. We are now able to write the semidiscrete formulation of the momentum equation with respect to the x_1-direction as

$$\begin{aligned}\frac{d}{dt}(\rho v_1)_i &= -\frac{1}{\mathrm{M}^2}p^{(0)}\underbrace{\sum_{j\in N(i)}\sum_{k=1}^{2} n_{ij,1}^k \left|l_{ij}^k\right|}_{=0} \\ &\quad -\frac{1}{\mathrm{M}}\sum_{j\in N(i)}\sum_{k=1}^{2}\left(\frac{p_i^{(1)} + p_j^{(1)}}{2} + \left(\frac{3p^{(0)}}{4c^{(0)}} + \eta_{ij}^{(0)}p^{(0)}\right)\Delta_{ij}v_{\mathbf{n}_{ij}^k}^{(0)}\right)n_{ij,1}^k\left|l_{ij}^k\right| + O(1), \quad \mathrm{M} \to 0.\end{aligned}$$

Now we are able to explore the first order pressure distribution by means of the perturbation equation of order $O\left(\mathrm{M}^{-1}\right)$, $\mathrm{M} \to 0$. With respect to the underlying discretization (see Figure 12) we get

$$p_k^{(1)} - p_\ell^{(1)} = \left(\frac{3p^{(0)}}{2c^{(0)}} + 2\eta_{i\ell}^{(0)}p^{(0)}\right)\Delta_{i\ell}v_1^{(0)} + \left(\frac{3p^{(0)}}{2c^{(0)}} + 2\eta_{ik}^{(0)}p^{(0)}\right)\Delta_{ik}v_1^{(0)}.$$

Due to the assumption (54) we obtain $0 < \eta_{i\ell}^{(0)} = \eta_{ik}^{(0)} =: \eta^{(0)}$ and consequently (55) yields

$$p_k^{(1)} - p_\ell^{(1)} = \underbrace{\left(\frac{3p^{(0)}}{2c^{(0)}} + 2\eta^{(0)}p^{(0)}\right)}_{>0}\underbrace{\left(v_{i,1}^{(0)} - v_{\ell,1}^{(0)} - v_{i,1}^{(0)} + v_{k,1}^{(0)}\right)}_{\neq 0} \neq 0. \tag{56}$$

This statement emphasizes that variations within the leading order velocity field can cause variations within the first order pressure distribution. These fluctuations are associated with the mesh size instead of the Mach number and thus we can state that this property contradicts the results of the continuous single as well as multiple length scale asymptotic analysis.

Note that the failure of the scheme due to variations within the first order pressure field can not be detected by such a kind of an asymptotic analysis which is based on the asymptotic sequence $\phi_n(\mathrm{M}) = \mathrm{M}^{2n}$.

It is remarkable that we didn't require any assumptions concerning the leading order velocity component $v_2^{(0)}$. Thus one can easily define a velocity distribution $\mathbf{v}$ such that the velocity field is divergence free in a discrete manner and satisfies the equation (55).

3.3. Numerical results for low Mach number flows

The statement concerning the spatial variations of the first order pressure distribution is based on a structured mesh and some quite theoretical assumptions (53), (54) and (55). Nevertheless, the results encourage the investigation of realistic flow fields to recognize these or somewhat related properties also within numerical simulations. Therefore, we consider the inviscid flow past the RAE2822 airfoil at varying freestream Mach numbers Ma_∞ between 10^{-6} and 0.1. From the isolines of the pressure distribution depicted in Figure 13 we suppose the unreliable and unphysical behaviour of the numerical method in the low Mach number regime. However, we have to point out the existence of the mentioned pressure fluctuations analytically. We close this gap by means of the indicator $\mathrm{Ind}(p)$ defined by equation (15). Thereby, the pressure p_i is considered to be located at the barycentre of the associated control volume σ_i and the indicator is evaluated in the obvious corresponding discrete manner.

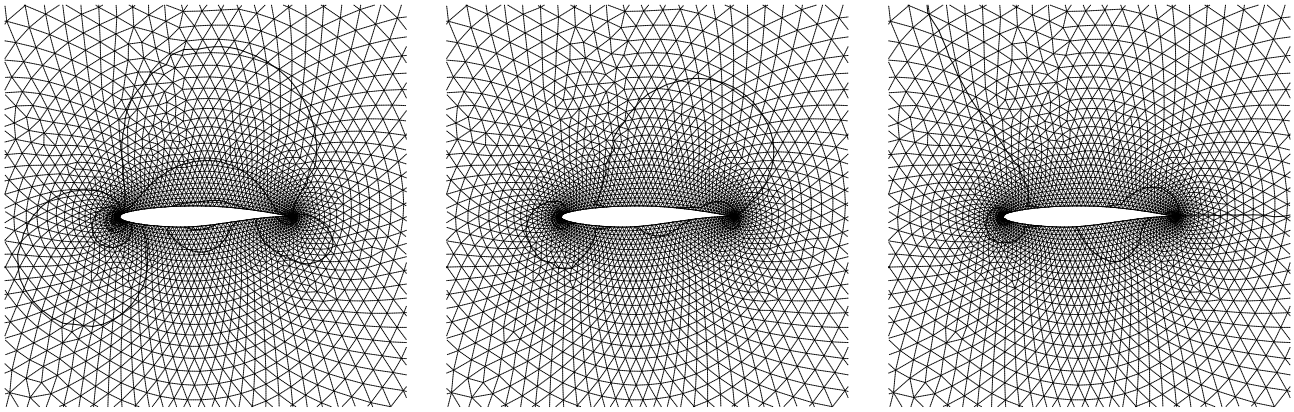

Figure 13: Isolines of the pressure distribution for varying freestream Mach numbers (10^{-1} (left), 10^{-2} (middle), 10^{-5} (right)) for the AUSMDV method

The solid line within diagram 14 represents $\mathrm{Ind}(p) = \mathrm{M}$. A comparison of the solid line with the results of the implicit as well as explicit finite volume scheme shows the unphysical behaviour

$$\mathrm{Ind}(p) = O(\mathrm{M}), \quad \mathrm{M} \to 0.$$

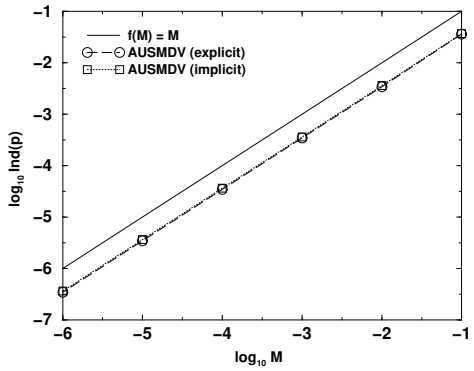

Figure 14: Pressure fluctuation $\mathrm{Ind}(p) = \dfrac{p_{\max} - p_{\min}}{p_{\max}\ \Delta \mathbf{x}_p}$ versus the Mach number for the AUSMDV scheme

4. Preconditioning

Preconditioning the governing equations was originally proposed by Chorin [7] and afterwards extended and systematically investigated by Turkel [71]. Chorin derived the preconditioned incompressible Navier-Stokes equations by adding a time-derivative of an arbitrary density function ρ to the divergence constraint and by simultaneously replacing the pressure inside the momentum equation by a likewise arbitrary equation of state $p = \rho/\delta$ with $\delta > 0$. Chorin mainly considered numerical aspects of the preconditioning technique by means of a finite difference method while Turkel described the influence of different preconditioners with respect to the characteristic propagation speeds of the system. Turkel suggested a quite simple preconditioner in the context of the compressible Euler equations formulated in terms of the entropy variables $\widetilde{\mathbf{w}} = (\widetilde{p}, v_1, v_2, \widetilde{s})^T$, whereby $\widetilde{s}$ denotes the entropy determined as $\widetilde{s} = \ln \frac{\widetilde{p}}{\widetilde{\rho}^{\gamma}}$.

Our purpose is now to carry over the preconditioning strategy into the current numerical framework. Therefore, we recast the governing equations (19) in their quasilinear form

$$\partial_t \widetilde{\mathbf{u}} + \sum_{\ell=1}^{2} \widetilde{\mathbf{F}}_\ell\,(\widetilde{\mathbf{u}})\,\partial_{x_\ell} \widetilde{\mathbf{u}} = \mathbf{0}, \tag{57}$$

where $\widetilde{\mathbf{F}}_\ell\,(\widetilde{\mathbf{u}})$, $\ell = 1, 2$, denote the Jacobian matrices of $\widetilde{\mathbf{f}}_\ell\,(\widetilde{\mathbf{u}})$, $\ell = 1, 2$, with respect to the conserved variables, i. e. $\widetilde{\mathbf{F}}_\ell\,(\widetilde{\mathbf{u}}) = \frac{\partial \widetilde{\mathbf{f}}_\ell}{\partial \widetilde{\mathbf{u}}}\,(\widetilde{\mathbf{u}})$.

Concerning the transformation of the governing equations we consider the matrices

$$\widetilde{\mathbf{W}}\left(\widetilde{\mathbf{u}}\right) = \frac{\partial \widetilde{\mathbf{w}}}{\partial \widetilde{\mathbf{u}}} \quad \text{and} \quad \widetilde{\mathbf{U}}\left(\widetilde{\mathbf{w}}\right) = \frac{\partial \widetilde{\mathbf{u}}}{\partial \widetilde{\mathbf{w}}}$$

which satisfy $\widetilde{\mathbf{U}}\left(\widetilde{\mathbf{w}}\right)\widetilde{\mathbf{W}}\left(\widetilde{\mathbf{u}}\right) = \mathbf{I}$. Multiplying (57) with $\widetilde{\mathbf{W}}\left(\widetilde{\mathbf{u}}\right)$ yields

$$\mathbf{0} = \partial_t \widetilde{\mathbf{w}} + \sum_{\ell=1}^{2} \widetilde{\mathbf{G}}_\ell\left(\widetilde{\mathbf{w}}\right) \partial_{x_\ell} \widetilde{\mathbf{w}}, \tag{58}$$

where

$$\widetilde{\mathbf{G}}_1\left(\widetilde{\mathbf{w}}\right) = \widetilde{\mathbf{W}}\left(\widetilde{\mathbf{u}}\right) \widetilde{\mathbf{F}}_1\left(\widetilde{\mathbf{u}}\right) \widetilde{\mathbf{U}}\left(\widetilde{\mathbf{w}}\right) = \begin{pmatrix} v_1 & \rho\widetilde{c}^2 & 0 & 0 \\ \frac{1}{\rho} & v_1 & 0 & 0 \\ 0 & 0 & v_1 & 0 \\ 0 & 0 & 0 & v_1 \end{pmatrix} \tag{59}$$

and

$$\widetilde{\mathbf{G}}_2\left(\widetilde{\mathbf{w}}\right) = \widetilde{\mathbf{W}}\left(\widetilde{\mathbf{u}}\right) \widetilde{\mathbf{F}}_2\left(\widetilde{\mathbf{u}}\right) \widetilde{\mathbf{U}}\left(\widetilde{\mathbf{w}}\right) = \begin{pmatrix} v_2 & 0 & \rho\widetilde{c}^2 & 0 \\ 0 & v_2 & 0 & 0 \\ \frac{1}{\rho} & 0 & v_2 & 0 \\ 0 & 0 & 0 & v_2 \end{pmatrix} \tag{60}$$

hold. The matrices $\widetilde{\mathbf{G}}_\ell$, $\ell = 1, 2$, reveal the weak coupling of the entropy equation with the velocity equations and the pressure equation. Due to that fact Turkel suggested to modify the velocity equations and the pressure equation whereas the entropy equation still remains unchanged. In a general formulation, the preconditioning can be written as

$$\mathbf{P}^{-1}\left(\widetilde{\mathbf{w}}\right) \partial_t \widetilde{\mathbf{w}} + \sum_{\ell=1}^{2} \widetilde{\mathbf{G}}_\ell\left(\widetilde{\mathbf{w}}\right) \partial_{x_\ell} \widetilde{\mathbf{w}} = \mathbf{0}, \tag{61}$$

where

$$\mathbf{P}^{-1}\left(\widetilde{\mathbf{w}}\right) = \begin{pmatrix} \frac{\widetilde{c}^2}{\zeta \mathrm{M}_\epsilon^2} & 0 & 0 & \delta \\ \frac{\alpha v_1}{\rho \zeta \mathrm{M}_\epsilon^2} & 1 & 0 & \delta \\ \frac{\alpha v_2}{\rho \zeta \mathrm{M}_\epsilon^2} & 0 & 1 & \delta \\ 0 & 0 & 0 & 1 \end{pmatrix}$$

with M_ϵ^2 chosen to be

$$\mathrm{M}_\epsilon^2 = \begin{cases} \epsilon^2 & , \quad \mathrm{M} < \epsilon \\ \mathrm{M}^2 & , \quad \epsilon \leq \mathrm{M} < 1 \\ 1 & , \quad \mathrm{M} \geq 1 \end{cases}$$

to ensure that the preconditioning matrix is always nonsingular. In this context the choice $\delta = 0$ leads to a class of preconditioners introduced by Turkel [71], whereas $\delta = 1$, $\alpha = 0$, and $\zeta = \widetilde{c}^2$ yields a method published by Choi and Merkle [6]. Although the matrix $\mathbf{P}^{-1}\left(\widetilde{\mathbf{w}}\right)$ is assumed to be nonsingular, it is obvious that a straightforward discretization of the governing equations (61) can be employed at most for the simulation of steady state phenomena. To overcome this fundamental restriction we follow Guillard and Viozat [14] and introduce a complete preconditioning of the governing equations in entropy form by

$$\mathbf{P}^{-1}\left(\widetilde{\mathbf{w}}\right) = \begin{pmatrix} \widetilde{\beta}^2 & 0 & 0 & 0 \\ 0 & 1 & 0 & 0 \\ 0 & 0 & 1 & 0 \\ 0 & 0 & 0 & 1 \end{pmatrix} \quad \text{with} \quad \widetilde{\beta} = O_S(\mathrm{M}), \quad \mathrm{M} \to 0.$$

As a result we obtain

$$\mathbf{0} = \mathbf{P}\left(\widetilde{\mathbf{w}}\right)\partial_t\widetilde{\mathbf{w}} + \sum_{\ell=1}^{2}\mathbf{P}\left(\widetilde{\mathbf{w}}\right)\widetilde{\mathbf{G}}_\ell\left(\widetilde{\mathbf{w}}\right)\partial_{x_\ell}\widetilde{\mathbf{w}} = \mathbf{P}\left(\widetilde{\mathbf{u}}\right)\partial_t\widetilde{\mathbf{u}} + \sum_{\ell=1}^{2}\widetilde{\mathbf{F}}_\ell^P\left(\widetilde{\mathbf{u}}\right)\partial_{x_\ell}\widetilde{\mathbf{u}}, \tag{62}$$

where

$$\mathbf{P}\left(\widetilde{\mathbf{u}}\right) = \widetilde{\mathbf{U}}\left(\widetilde{\mathbf{w}}\right)\mathbf{P}\left(\widetilde{\mathbf{w}}\right)\widetilde{\mathbf{W}}\left(\widetilde{\mathbf{u}}\right) = \mathbf{I} + (\widetilde{\beta}^2 - 1)\frac{\gamma-1}{\widetilde{c}^2}\begin{pmatrix} \frac{|\mathbf{v}|^2}{2} & -v_1 & -v_2 & 1 \\ \frac{|\mathbf{v}|v_1}{2} & -v_1^2 & -v_1v_2 & v_1 \\ \frac{|\mathbf{v}|v_2}{2} & -v_1v_2 & -v_2^2 & v_2 \\ \frac{|\mathbf{v}|\widetilde{H}}{2} & -\widetilde{H}v_1 & -\widetilde{H}v_2 & \widetilde{H} \end{pmatrix}$$

and $\widetilde{\mathbf{F}}_\ell^P\left(\widetilde{\mathbf{u}}\right) = \mathbf{P}\left(\widetilde{\mathbf{u}}\right)\widetilde{\mathbf{F}}_\ell\left(\widetilde{\mathbf{u}}\right)$, $\ell = 1, 2$. Note that system (62) is equivalent to (57) and (56) for all $\mathrm{M} > 0$.

In order to enable a flawless computation of flow fields at arbitrary speeds we combine the AUSMDV method with a preconditioned formulation of the Lax-Friedrichs scheme such that the advantageous properties of the AUSMDV flux function for transsonic, supersonic, and hypersonic fluid flow will be tied together with the asymptotic validity of the preconditioned Lax-Friedrichs method in the low Mach number regime.

Numerical flux functions of Lax-Friedrichs type usually differ from the dissipation term $\widetilde{\mathbf{D}}\left(\widetilde{\mathbf{z}}_R - \widetilde{\mathbf{z}}_L\right)$. With respect to the governing equations (19) Hu and Shu [29] defined $\widetilde{\mathbf{D}} \in \mathbb{R}$ to be the largest absolute eigenvalue of the corresponding Jacobian matrix $\widetilde{\mathbf{F}}\left(\widetilde{\mathbf{z}}; \mathbf{n}\right)$. Similar to the formulation of Shu and Osher [62] we prefer a matrix-valued term $\widetilde{\mathbf{D}}$ which was recently proposed by Friedrich [10].

Using the abbreviations

$$\xi_1 = \lambda_3^P - \lambda_1^P\widetilde{\beta}^2, \quad \xi_2 = \lambda_4^P - \lambda_1^P\widetilde{\beta}^2, \quad \text{and} \quad \xi_3 = \frac{\lambda_4^P - \lambda_3^P}{2} \tag{63}$$

the matrix of the right eigenvectors of $\widetilde{\mathbf{F}}^P\left(\widetilde{\mathbf{u}}; \mathbf{n}\right)$ reads

$$\widetilde{\mathbf{R}}^P\left(\widetilde{\mathbf{u}}; \mathbf{n}\right) = \begin{pmatrix} \frac{(\gamma-1)|\mathbf{v}|^2}{2\widetilde{p}} - \frac{\gamma}{\rho} & -\frac{(\gamma-1)v_1}{\widetilde{p}} & -\frac{(\gamma-1)v_2}{\widetilde{p}} & \frac{\gamma-1}{\widetilde{p}} \\ -\frac{v_{\mathbf{t}}}{\rho} & -\frac{n_2}{\rho} & -\frac{n_1}{\rho} & 0 \\ \frac{(\gamma-1)\xi_2|\mathbf{v}|^2 + 2\widetilde{\beta}^2\widetilde{c}^2v_{\mathbf{n}}}{4\xi_3} & -\frac{(\gamma-1)\xi_2v_1 + \widetilde{\beta}^2\widetilde{c}^2n_1}{2\xi_3} & -\frac{(\gamma-1)\xi_2v_2 + \widetilde{\beta}^2\widetilde{c}^2n_2}{2\xi_3} & \frac{(\gamma-1)\xi_2}{2\xi_3} \\ -\frac{(\gamma-1)\xi_1|\mathbf{v}|^2 + 2\widetilde{\beta}^2\widetilde{c}^2v_{\mathbf{n}}}{4\xi_3} & \frac{(\gamma-1)\xi_1v_1 + \widetilde{\beta}^2\widetilde{c}^2n_1}{2\xi_3} & \frac{(\gamma-1)\xi_1v_2 + \widetilde{\beta}^2\widetilde{c}^2n_2}{2\xi_3} & -\frac{(\gamma-1)\xi_1}{2\xi_3} \end{pmatrix}.$$

Hence the Jacobian matrix can be expressed as

$$\widetilde{\mathbf{F}}^P\left(\widetilde{\mathbf{u}}; \mathbf{n}\right) = \widetilde{\mathbf{R}}^P\left(\widetilde{\mathbf{u}}; \mathbf{n}\right)\widetilde{\Lambda}^P\left(\widetilde{\mathbf{u}}; \mathbf{n}\right)\left(\widetilde{\mathbf{R}}^P\right)^{-1}\left(\widetilde{\mathbf{u}}; \mathbf{n}\right),$$

where $\widetilde{\Lambda}^P\left(\widetilde{\mathbf{u}}; \mathbf{n}\right) = \mathrm{diag}\left\{\lambda_1^P\left(\widetilde{\mathbf{u}}; \mathbf{n}\right), \ldots, \lambda_4^P\left(\widetilde{\mathbf{u}}; \mathbf{n}\right)\right\} \in \mathbb{R}^{4\times4}$ consists of the eigenvalues

$$\lambda_{1/2}^P\left(\widetilde{\mathbf{u}}; \mathbf{n}\right) = v_{\mathbf{n}} \quad \text{and} \quad \lambda_{3/4}^P\left(\widetilde{\mathbf{u}}; \mathbf{n}\right) = \frac{1}{2}\left(\left(1 + \widetilde{\beta}^2\right)v_{\mathbf{n}} \pm \sqrt{((1-\widetilde{\beta}^2)v_{\mathbf{n}})^2 + 4\widetilde{\beta}^2\widetilde{c}^2}\right).$$

Following the proceeding of Friedrich [10] we obtain the preconditioned Lax-Friedrichs scheme in the form

$$\mathbf{H}^{LF(P)}\left(\widetilde{\mathbf{z}}_L, \widetilde{\mathbf{z}}_R; \mathbf{n}\right) = \frac{1}{2}\left(\mathbf{T}^{-1}(\mathbf{n})\left\{\widetilde{\mathbf{f}}_1\left(\mathbf{T}(\mathbf{n})\widetilde{\mathbf{z}}_L\right) + \widetilde{\mathbf{f}}_1\left(\mathbf{T}(\mathbf{n})\widetilde{\mathbf{z}}_R\right)\right\} - \widetilde{\mathbf{D}}^P\left(\widetilde{\mathbf{z}}_L, \widetilde{\mathbf{z}}_R; \mathbf{n}\right)\left(\widetilde{\mathbf{z}}_R - \widetilde{\mathbf{z}}_L\right)\right), \tag{64}$$

where the dissipation matrix is defined to be

$$\widetilde{\mathbf{D}}^P\left(\widetilde{\mathbf{z}}_L, \widetilde{\mathbf{z}}_R; \mathbf{n}\right) = \mathbf{P}^{-1}\left(\frac{\widetilde{\mathbf{z}}_L + \widetilde{\mathbf{z}}_R}{2}\right)\widetilde{\mathbf{R}}^P\left(\frac{\widetilde{\mathbf{z}}_L + \widetilde{\mathbf{z}}_R}{2}; \mathbf{n}\right)\left|\widetilde{\Lambda}^P\right|\left(\widetilde{\mathbf{z}}_L, \widetilde{\mathbf{z}}_R; \mathbf{n}\right)\left(\widetilde{\mathbf{R}}^P\right)^{-1}\left(\frac{\widetilde{\mathbf{z}}_L + \widetilde{\mathbf{z}}_R}{2}; \mathbf{n}\right)$$

with

$$\left|\widetilde{\Lambda}^P\right|\left(\widetilde{\mathbf{z}}_L, \widetilde{\mathbf{z}}_R; \mathbf{n}\right) = \mathrm{diag}\left\{\max_{\mathbf{z}\in\left\{\widetilde{\mathbf{z}}_L, \widetilde{\mathbf{z}}_R, \frac{\widetilde{\mathbf{z}}_L + \widetilde{\mathbf{z}}_R}{2}\right\}}\left|\lambda_1^P(\mathbf{z}; \mathbf{n})\right|, \ldots, \max_{\mathbf{z}\in\left\{\widetilde{\mathbf{z}}_L, \widetilde{\mathbf{z}}_R, \frac{\widetilde{\mathbf{z}}_L + \widetilde{\mathbf{z}}_R}{2}\right\}}\left|\lambda_4^P(\mathbf{z}; \mathbf{n})\right|\right\}.$$

Note that the preconditioned Lax-Friedrichs scheme represents a consistent numerical flux function with respect to the Euler equations and the difference between the standard method and the preconditioned algorithm is exclusively contained in the dissipation term. Hence, the preconditioned method is suitable for the simulation of steady as well as unsteady flow fields.

4.1. Asymptotic analysis

Since the principle procedure of a discrete asymptotic analysis was extensively explained in Section 3.2, it is possible to derive the important results concerning the preconditioned numerical method in a brief manner.

In order to obtain a compact formulation of the dissipation term we introduce the following auxiliary values

$$\eta_1 = \left(1 - \mathrm{M}^2 \frac{(\gamma-1)|\mathbf{v}|^2}{c^2}\right) \Delta_{ji}\rho + \mathrm{M}^2 \frac{(\gamma-1)v_1}{c^2}\Delta_{ji}m_1 + \mathrm{M}^2 \frac{(\gamma-1)v_2}{c^2}\Delta_{ji}m_2 - \frac{\gamma-1}{c^2}\Delta_{ji}(\rho E), \tag{65}$$

$$\begin{aligned}\eta_2 = &\left(\xi_2 \frac{(\gamma-1)|\mathbf{v}|^2}{2} + \mathrm{M}^2\beta^2c^2v_{\mathbf{n}}\right)\Delta_{ji}\rho - \left(\xi_2(\gamma-1)v_1 + \mathrm{M}^2\beta^2c^2n_1\right)\Delta_{ji}m_1 \\ &- \left(\xi_2(\gamma-1)v_2 + \mathrm{M}^2\beta^2c^2n_2\right)\Delta_{ji}m_2,\end{aligned} \tag{66}$$

$$\begin{aligned}\eta_3 = &-\left(\xi_1 \frac{(\gamma-1)|\mathbf{v}|^2}{2} + \mathrm{M}^2\beta^2c^2v_{\mathbf{n}}\right)\Delta_{ji}\rho + \left(\xi_1(\gamma-1)v_1 + \mathrm{M}^2\beta^2c^2n_1\right)\Delta_{ji}m_1 \\ &+ \left(\xi_1(\gamma-1)v_2 + \mathrm{M}^2\beta^2c^2n_2\right)\Delta_{ji}m_2,\end{aligned} \tag{67}$$

and

$$\eta_4 = \frac{1}{2\beta^2c^2\xi_3}, \tag{68}$$

where $\beta = \frac{|\widetilde{\beta}|}{\mathrm{M}} = O_S(1)$, $\mathrm{M} \to 0$, and the physical quantities φ which are occurring without an index i or j (φ_i or $\Delta_{ji}\varphi$) are defined to be the average of φ_i and φ_j, i. e. $\varphi = \frac{\varphi_i+\varphi_j}{2}$.

By means of the above mentioned values the dissipation term of the numerical mass flux reads

$$\widetilde{\mathbf{D}}_\rho\left(\widetilde{\mathbf{u}}_i, \widetilde{\mathbf{u}}_j; \mathbf{n}\right)\Delta_{ji}\widetilde{\mathbf{u}} = \left|\lambda_1^P\right|\eta_1 + \eta_4\left\{\left|\lambda_3^P\right|\eta_2 + \left|\lambda_4^P\right|\eta_3 + \frac{\gamma-1}{\mathrm{M}^2}\Big(\left|\lambda_3^P\right|\xi_2 - \left|\lambda_4^P\right|\xi_1\Big)\Delta_{ji}(\rho E)\right\}, \tag{69}$$

where $\left|\lambda_k^P\right|$ represents the k-th diagonal term of the matrix $\left|\widetilde{\Lambda}^P\right|$ [47].

To assess the influence of the Mach number we separately explore the terms inside the numerical dissipation (69). It is obvious from the consideration of the eigenvalue $\lambda_1^P = v_{\mathbf{n}}$ and the equation (65) that $\left|\lambda_1^P\right|\eta_1 = O(1)$, $\mathrm{M} \to 0$. Furthermore, the variable ξ_3 satisfies

$$\xi_3 = -\frac{1}{2}\sqrt{\left(1-\mathrm{M}^2\beta^2\right)^2 v_{\mathbf{n}}^2 + 4\beta^2c^2} = \underbrace{-\frac{1}{2}\sqrt{v_{\mathbf{n}}^2 + 4\beta^2c^2}}_{=d_{ij}<0} + O\left(\mathrm{M}^2\right), \quad \mathrm{M} \to 0. \tag{70}$$

As a straightforward consequence we obtain

$$\eta_4 = \underbrace{\frac{1}{2\beta^2c^2d_{ij}}}_{=a_{ij}<0} + O\left(\mathrm{M}^2\right), \quad \mathrm{M} \to 0. \tag{71}$$

In the case that the Mach number M is sufficiently small one gets $c^2 > \mathrm{M}^2v_{\mathbf{n}}^2$ by which it follows that

$$\left(1-\mathrm{M}^2\beta^2\right)^2 v_{\mathbf{n}}^2 + 4\beta^2c^2 > \left(1+\mathrm{M}^2\beta^2\right)^2 v_{\mathbf{n}}^2.$$

This equation yields $\lambda_3^P > 0$, $\lambda_4^P < 0$ and consequently

$$\left|\lambda_3^P\right|\xi_2 - \left|\lambda_4^P\right|\xi_1 = \left|\lambda_3^P\right|\lambda_4^P - \left|\lambda_4^P\right|\lambda_3^P + O\left(\mathrm{M}^2\right) = \underbrace{b_{ij}}_{<0} + O\left(\mathrm{M}^2\right), \quad \mathrm{M} \to 0. \tag{72}$$

Taking account $\left|\lambda_3^P\right|\eta_2 - \left|\lambda_4^P\right|\eta_3 = O(1)$, $\mathrm{M} \to 0$, as well as $(\rho_i \mathbf{v}_i + \rho_j \mathbf{v}_j)\mathbf{n} = O(1)$, $\mathrm{M} \to 0$, in combination with (71), (72) and $\rho E = \frac{p}{\gamma - 1} + O\left(\mathrm{M}^2\right)$, $\mathrm{M} \to 0$, results in

$$\mathbf{H}_{\rho}^{LF(P)}\left(\widetilde{\mathbf{u}}_i, \widetilde{\mathbf{u}}_j; \mathbf{n}\right) = \frac{1}{\mathrm{M}^2} a_{ij} b_{ij} \frac{\Delta_{ji} p}{2} + O(1), \quad \mathrm{M} \to 0.$$

Introducing the asymptotic expansion (46) and identifying terms multiplied by the same power of the Mach number yields the perturbation equations

$$0 = \sum_{j \in N(i)} \sum_{k=1}^{2} \left(a_{ij} b_{ij}\right)^{(0)} \frac{\Delta_{ji} p^{(0)}}{2} \left|l_{ij}^k\right| + \vartheta_i \left(a_{i\infty} b_{i\infty}\right)^{(0)} \frac{\Delta_{\infty i} p^{(0)}}{2} \left|l_{\sigma_i}\right| \tag{73}$$

and

$$\begin{aligned} 0 = & \sum_{j \in N(i)} \sum_{k=1}^{2} \left(\left(a_{ij} b_{ij}\right)^{(0)} \frac{\Delta_{ji} p^{(1)}}{2} + \left(a_{ij} b_{ij}\right)^{(1)} \frac{\Delta_{ji} p^{(0)}}{2} \right) \left|l_{ij}^k\right| \\ & + \vartheta_i \left(\left(a_{i\infty} b_{i\infty}\right)^{(0)} \frac{\Delta_{\infty i} p^{(1)}}{2} + \left(a_{i\infty} b_{i\infty}\right)^{(1)} \frac{\Delta_{\infty i} p^{(0)}}{2} \right) \left|l_{\sigma_i}\right|, \end{aligned} \tag{74}$$

where

$$\left(a_{ij} b_{ij}\right)^{(0)} = \lim_{\mathrm{M} \to 0} \left(a_{ij} b_{ij}\right) > 0. \tag{75}$$

Corresponding to the argumentation employed in Section 3.2 (see equations (51) and (52)) the statements (73) and (75) prove that variations within the discrete pressure field are at most of order M, i. e. the numerical method always computes a spatially homogeneous leading order pressure distribution. Thus, equation (74) degenerates to

$$0 = \sum_{j \in N(i)} \sum_{k=1}^{2} \left(a_{ij} b_{ij}\right)^{(0)} \frac{\Delta_{ji} p^{(1)}}{2} \left|l_{ij}^k\right| + \vartheta_i \left(a_{i\infty} b_{i\infty}\right)^{(0)} \frac{\Delta_{\infty i} p^{(1)}}{2} \left|l_{\sigma_i}\right|. \tag{76}$$

Comparing (76) with (73) obviously establishes that the first order pressure field $p^{(1)}$ is likewise spatially constant in agreement with the continuous single length scale asymptotic analysis.

4.2. Low Mach number simulations

As mentioned above, the final version of the numerical flux function is obtained by means of a combination of $\mathbf{H}^{AUSMDV}$ and $\mathbf{H}^{LF(P)}$. Thus, we determine

$$\mathbf{H}\left(\widetilde{\mathbf{z}}_L, \widetilde{\mathbf{z}}_R; \mathbf{n}\right) = \delta \mathbf{H}^{AUSMDV}\left(\widetilde{\mathbf{z}}_L, \widetilde{\mathbf{z}}_R; \mathbf{n}\right) + (1 - \delta) \mathbf{H}^{LF(P)}\left(\widetilde{\mathbf{z}}_L, \widetilde{\mathbf{z}}_R; \mathbf{n}\right), \tag{77}$$

where

$$\delta = \begin{cases} 1 & , \text{ if } \widetilde{\mathrm{Ma}}_{\infty} > 0.1 \text{ or } \widetilde{\mathrm{Ma}}_{LR} = \frac{|\mathbf{v}_L + \mathbf{v}_R|}{\widetilde{c}_L + \widetilde{c}_R} > 0.1 \\ 0 & , \text{ otherwise.} \end{cases}$$

Using the function $g(\mathrm{M}) = \sum_{k=0}^{3} a_k \mathrm{M}^k$ with $a_0 = 4.997$, $a_1 = -239.86$, $a_2 = 3598.1$ and $a_3 = -15992$ the parameter $\widetilde{\beta}^2$ is defined to be

$$\widetilde{\beta}^2 = \begin{cases} 0.1\epsilon^2 & , \text{ if } \widetilde{\mathrm{Ma}}_{LR} < \epsilon, \\ 0.1\widetilde{\mathrm{Ma}}_{LR}^2 & , \text{ if } \epsilon \leq \widetilde{\mathrm{Ma}}_{LR} < 0.05, \\ g\left(\widetilde{\mathrm{Ma}}_{LR}\right) & , \text{ if } 0.05 \leq \widetilde{\mathrm{Ma}}_{LR} < 0.1, \\ 1 & , \text{ if } \widetilde{\mathrm{Ma}}_{LR} \geq 0.1. \end{cases}$$

Note that the threshold value $\epsilon > 0$ depends on the arithmetic accuracy of the computer and should be chosen as small as possible.

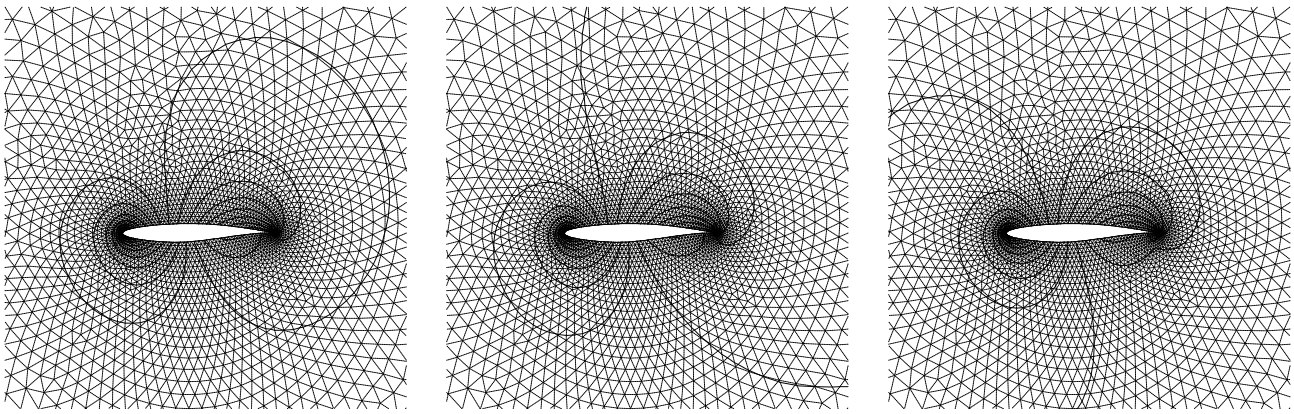

Figure 15: Isolines of the pressure distribution for varying Mach numbers (10^{-2} (left), 10^{-4} (middle), 10^{-5} (right)) for the preconditioned method (77)

Since the validity and reliability of this method in the context of transsonic, supersonic and hypersonic flow fields was proven in Section we can currently focus our attention to low Mach number fluid flow. Thus, we consider exactly the same test case as used in Section 3.3.

The isolines of the pressure distribution depicted in Figure 15 indicate that the derive finite volume method is convenient also for the simulation of low speed flow. Nevertheless, an evidence concerning the asymptotic correctness of the computed pressure field is demonstrably given by Figure 16. The results confirm $\mathrm{Ind}(p) = O\left(\mathrm{M}^2\right)$, $\mathrm{M} \to 0$, which coincides with the continuous as well as with the discrete asymptotic analysis.

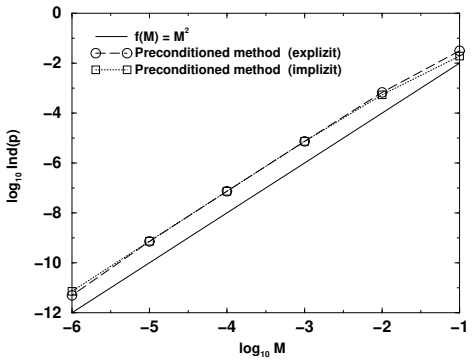

Figure 16: Pressure fluctuation $\mathrm{Ind}(p) = \dfrac{p_{\max} - p_{\min}}{p_{\max}\ \Delta \mathbf{x}_p}$ versus the Mach number for the preconditioned method (77)

5. Conclusion and outlook

A finite volume approximation of the Euler equations of gas dynamics using the AUSMDV scheme is presented, whereby the stability and high resolution properties of the method in the field of trans-, super-, and hypersonic inviscid fluid flow are proved by means of several realistic test cases from engineering.

The results of a single as well as multiple scale asymptotic analysis are used as a guideline to judge the behaviour of the numerical method in the low Mach number regime. Since the AUSMDV method fails for low speed flows, a combination of this numerical flux function with a preconditioned formulation of the Lax-Friedrichs scheme is developed. The validity of this approach with respect to the computed pressure distribution is established by means of an asymptotic analysis as well as numerical experiments.

A proof concerning the divergence constraint of the discrete velocity field is still missing. The closure of this gap probably requires some additional modifications of the numerical method and will be the topic of future research. Moreover, the extension of this method to viscous fluid flow will be presented in a forthcoming paper.

Acknowledgments

The author is grateful to Prof. Dr. R. Ansorge for initiating this paper as well as to Prof. Dr. H. Schwetlick for his invitation. The author furthermore would like to express his thanks to Prof. Dr. Th. Sonar for years of fruitful collaboration in the field of finite volume methods on unstructured grids. Moreover, the author is indebted to Dr. N. Botta, Dr. L. Hoffmann, Prof. Dr. R. Klein, Prof. Dr. C.-D. Munz and Dr. S. Roller for numerous valuable discussions. Last but not least I would like to thank Dr. M. Breuß for proof reading the manuscript.

References

[1] J. D. Anderson. *Hypersonic and high temperature gas dynamics.* MacGraw-Hill, Series in aeronautical and aerospace engineering, Singapore, 1989.

[2] K. Asano. On the Incompressible Limit of the Compressible Euler Equations. *Japan J. Appl. Math.*, 4: 455–488, 1987.

[3] O. Axelsson. *Iterative Solution Methods.* Cambridge University Press, Cambridge, 1996.

[4] T. J. Barth, D. C. Jesperson. The Design and Application of Upwind Schemes on Unstructured Meshes. *AIAA paper*, 89–0366, 1989.

[5] W. R. Briley, H. McDonald, S. J. Shamroth. A Low Mach Number Euler Formulation and Application to Time-Iterative LBI Schemes. *AIAA J.*, 21 (10): 1467–1469, 1983.

[6] D. Choi, C. L. Merkle. The Application of Preconditioning in Viscous Flows. *J. Comput. Phys.*, 105: 207–223, 1993.

[7] A. J. Chorin. A Numerical Method for Solving Incompressible Viscous Flow Problems. *J. Comput. Phys.*, 2: 12–26, 1967.

[8] A. Erdélyi. *Asymptotic Expansions.* Dover Publications, New York, 1956.

[9] O. Friedrich. Weighted Essential Non-Oscillatory Schemes for the Interpolation of Mean Values on Unstructured Grids. *J. Comput. Phys.*, 144: 194–212, 1998.

[10] O. Friedrich. *Gewichtete wesentlich nicht-oszillierende Verfahren auf unstrukturierten Gittern.* Dissertation, Fachbereich Mathematik, Schwerpunkt Differentialgleichungen und Dynamische Systeme, Universität Hamburg, 1999.

[11] O. Friedrich, D. Hempel, A. Meister, Th. Sonar. Adaptive Computation of Unsteady Flow Fields with the DLR-$\mathcal{T}$-Code. in: 77th AGARD Fluid Dynamics Panel Meeting and Symposium on Progress and Challenges in CFD Methods and Algorithms, AGARD-CP-578, Sevilla, 1995.

[12] E. Godlewski, P.-A. Raviart. *Numerical Approximation of Hyperbolic Systems of Conservation Laws*, volume 118 of *Applied Mathematical Sciences.* Springer, New York, Berlin, Heidelberg, 1996.

[13] S. K. Godunov. A Finite Difference Method for the Numerical Computation of Discontinuous Solutions of the Equations of Fluid Dynamics. *Mat. Sb.*, 47: 357–393, 1959.

[14] H. Guillard, C. Viozat. On the Behaviour of Upwind Schemes in the Low Mach Number Limit. *Computers and Fluids*, Vol. 28: 63–86, 1999.

[15] W. Hackbusch. *Iterative Lösung großer schwachbesetzter Gleichungssysteme.* Teubner, Stuttgart, 2., überarb. und erw. edition , 1993.

[16] D. Hänel, R. Schwane. An implicit flux-vector splitting scheme for the computation of viscous hypersonic flow. *AIAA Paper*, 89–0274, 1989.

[17] D. Hänel, R. Schwane, G. Seider. On the accuracy of upwind schemes for the solution of the navier-stokes equations. *AIAA Paper*, 87–1105, 1987.

[18] V. Hannemann. *Numerische Simulation von Stoß-Stoß-Wechselwirkungen unter Berücksichtigung von chemischen und thermischen Nichtgleichgewichtseffekten.* Dissertation, Universität Göttingen, 1996.

[19] V. Hannemann, D. Hempel, Th. Sonar. Dynamic Adaptivity and Residual Control in Unsteady Compressible Flow Computation. *Mathematical and Computer Modelling*, 20: 201–213, 1994.

[20] G. Hauke, T. J. R. Hughes. A Comparative Study of Different Sets of Variables for Solving Compressible and Incompressible Flows. *Comput. Methods Appl. Mech. Engrg*, 153: 1–44, 1998.

[21] B. Heinrich. *Finite Difference Methods on Irregular Networks.* Birkhäuser Verlag, Basel, 1987.

[22] D. Hietel, A. Meister, Th. Sonar. On the comparison of four different implementations of an third-order ENO scheme of box type for the computation of compressible flow. *Numerical Algorithms*, 13: 77–105, 1996.

[23] C. Hirsch. *Numerical computation of internal and external flows*, volume 1. Wiley & Sons, Chicester, New York, 1988.

[24] C. Hirsch. *Numerical computation of internal and external flows*, volume 2. Wiley & Sons, Chicester, New York, 1988.

[25] L. Hoffmann. *Ein zeitlich selbstadaptives numerisches Verfahren zur Berechnung von Strömungen aller Mach-Zahlen basierend auf Mehrskalenasymptotik und diskreter Datenanalyse.* Dissertation, Fachbereich Mathematik, Schwerpunkt Differentialgleichungen und Dynamische Systeme, Universität Hamburg, 2000.

[26] L. Hoffmann, A. Meister. A Numerical Scheme for Low Mach Number Flow based on Asymptotic Analysis with Time-Dependent Adaptation of the Asymptotic Sequence. In *Proceedings of the Fourth ECCOMAS Computational Fluid Dynamics Conference*, (Eds.) C. Hirsch, et. al. Pandolfi, M., volume 1, Part 1, pp. 567–572, Athens, 1998.

[27] L. Hoffmann, A. Meister. The Extension of a Compressible Flow Solver to the Low Mach Number Regime. In *Proceedings of the 3nd Seminar on Euler and Navier-Stokes Equations*, Prague, 1998.

[28] L. Hoffmann, A. Meister. A Compressible Low Mach Number Scheme based on Image Processing and Asymptotic Analysis. *Computational Fluid Dynamics Journal*, Vol. 9: 231–242, 2001.

[29] C. Hu, C.-W. Shu. Weighted Essentially Non-oscillatory Schemes on Triangular Meshes. *J. Comput. Phys.*, 150: 97–127, 1999.

[30] A. Jameson. Computational Transonics. *Comm. Pure Appl. Math.*, 41: 507–549, 1988.

[31] J. Kevorkian, J. D. Cole. *Multiple Scale and Singular Perturbation Methods*, volume 114 of *Applied Mathematical Sciences.* Springer, New York, Berlin, Heidelberg, 1996.

[32] S. Klainerman, A. Majda. Singular limits of quasilinear hyperbolic system with large parameters and the incompressible limit of compressible fluids. *Comm. Pure Appl. Math.*, 34: 481–524, 1981.

[33] S. Klainerman, A. Majda. Compressible and incompressible fluids. *Comm. Pure Appl. Math.*, 35: 629–651, 1982.

[34] R. Klein. Semi-Implicit Extension of a Godunov-Type Scheme Based on Low Mach Number Asymptotics I: One-Dimensional Flow. *J. Comput. Phys.*, 121: 213–237, 1995.

[35] R. Klein, N. Botta, T. Schneider, C.D. Munz, S. Roller, A. Meister, L. Hoffmann, Th. Sonar. Asymptotic adaptive methods for multi-scale problems in fluid mechanics. *Journal of Engineering Mathematics*, Vol. 9 (1/4) (2): 261–343, 2001.

[36] N. Kroll, R.K. Jain. Solution of Two-Dimensional Euler Equations — Experience with a Finite Volume Code. Deutsche Forschungs- und Versuchsanstalt für Luft- und Raumfahrt DFVLR, Forschungsbericht FB 87-41, Köln, 1987.

[37] D. Kröner. *Numerical Schemes for Conservation Laws.* Teubner, Stuttgart, 1997.

[38] J. L. Latecki, R. Lakämper. Polygon Evolution by Vertex Deletion. In *2nd Int. Conf. on Scale-Space Theories in Computer Vision*, pp. 398–409, Corfu, Greece, 1999. Springer-Verlag.

[39] L. J. Latecki, R. Lakämper. Convexity Rule for Shape Decomposition Based on Discrete Contour Evolution. *Comput. Vision Image Understanding*, 73 (3): 441–454, 1999.

[40] R. J. LeVeque. *Numerical Methods for Conservation Laws.* Birkhäuser, Basel, 1990.

[41] M.-S. Liou, C.J. Steffen. A New Flux Splitting Scheme. NASA Technical Memorandum 104404, Cleveland, Ohio, May 1991. also in J. Comput. Phys. **107**, 23–39, 1993.

[42] A. Meister. Development of an Implicit Finite Volume Scheme for the Computation of Unsteady Flow Fields on Unstructured Moving Grids. In *Numerical Methods for Fluid Dynamics V*, pp. 481–488, Oxford, 1995. Clarendon Press. Ed. K.W. Morton and M.J. Baines.

[43] A. Meister. *Zur zeitgenauen numerischen Simulation reibungsbehafteter, kompressibler, turbulenter Strömungsfelder mit einer impliziten Finite-Volumen-Methode vom Box-Typ.* Dissertation, Technische Hochschule Darmstadt, 1996.

[44] A. Meister. Comparison of Different Krylov Subspace Methods Embedded in an Implicit Finite Volume Scheme for the Computation of Viscous and Inviscid Flow Fields on Unstructured Grids. *J. Comput. Phys.*, 140: 311–345, 1998.

[45] A. Meister. Asymptotic Single and Multiple Scale Expansions in the Low Mach Number Limit. *SIAM J. Appl. Math.*, Vol. 60 (1): 256–271, 1999.

[46] A. Meister. *Numerik linearer Gleichungssysteme, Eine Einführung in moderne Verfahren.* Vieweg, Wiesbaden, 1999.

[47] A. Meister. Analyse und Anwendung Asymptotik-basierter numerischer Verfahren zur Simulation reibungsbehafteter Strömungen in allen Mach-Zahlbereichen, 2001. Habilitationsschrift, Universität Hamburg.

[48] A. Meister, M. Oevermann. Computation of Laminar and Turbulent Compressible Flow Fields on Unstructured Grids with an Implicit Finite Volume Scheme. In *Proceedings of the 2nd Seminar on Euler and Navier-Stokes Equations*, Prague, 1996.

[49] A. Meister, M. Oevermann. An Implicit Finite Volume Approach of the $k-\epsilon$ Turbulence Model on Unstructured Grids. *Z. Angew. Math. Mech.*, 78 (11): 743–757, 1998.

[50] A. Meister, Th. Sonar. Finite-volume schemes for compressible fluid flow. *Surv. Math. Ind.*, 8: 1–36, 1998.

[51] A. Meister, C. Vömel. Efficient Preconditioning of Linear Systems arising from the Discretization of Hyperbolic Conservation Laws. *Advances in Computational Mathematics*, Vol.14 (1): 49–73, 2001.

[52] C. L. Merkle, Y.-H. Choi. Computation of Low-Speed Compressible Flows with Heat Addition. *AIAA J.*, 25 (6): 831–838, 1987.

[53] C. L. Merkle, Y.-H. Choi. Computation of Low-Speed Compressible Flows with Time-Marching Procedure. *Int. J. Num. Meth. Eng.*, Vol. 25: 293–311, 1988.

[54] S. Osher, F. Solomon. Upwind Schemes for Hyperbolic Systems of Conservation Laws. *Math. Comput.*, 38: 339–377, 1982.

[55] J. J. Quirk. A Contribution to the Great Riemann Solver Debate. ICASE Report 92–64, Hampton, Virginia, 1992.

[56] (Eds.) A. Rizzi, H. Viviand. *Numerical Methods for the Computation of Inviscid Transonic Flows with Shock Waves*, number 3 in Notes on Numerical Fluid Mechanics, Braunschweig, Wiesbaden, 1981. Vieweg.

[57] P. L. Roe. Approximate Riemann Solvers, Parameter Vectors, and Difference Schemes. *J. Comput. Phys.*, 43: 357–372, 1981.

[58] Y. Saad. *Iterative Methods for Sparse Linear Systems.* PWS Publishing Company, Boston, 1996.

[59] T. Schneider, N. Botta, K. J. Geratz, R. Klein. Semi-Implicit Extension of a Godunov-Type Compressible Solver Based on Low Mach Number Asymptotics II: Multi-Dimesional, Variable Density Zero Mach Number Flow. *J. Comput. Phys.*, 155: 248–286, 1999.

[60] W. Schneider. *Mathematische Methoden der Strömungsmechanik.* Vieweg, Braunschweig, 1987.

[61] J. Sesterhenn. *Zur numerischen Berechnung kompressibler Strömungen bei kleinen Mach-Zahlen.* PhD thesis, Swiss Federal Institute of Technology, Diss. ETH No. 11334, 1995.

[62] C.-W. Shu, S. Osher. Efficient Implementation of Essentially Nonoscillatory Shock-Capturing Schemes. *J. Comput. Phys.*, 77: 439–471, 1988.

[63] J.-S. Shuen, K.-H. Chen, Y. Choi. A Coupled Implicit Method for Chemical Non-equilibrium Flows at All Speeds. *J. Comput. Phys.*, 106: 306–318, 1993.

[64] Th. Sonar. On the Design of an Upwind Scheme for Compressible Flow on General Triangulations. *Numerical Algorithms*, 4: 135–149, 1993.

[65] Th. Sonar. *Mehrdimensionale ENO-Verfahren.* Teubner Verlag, Stuttgart, 1997.

[66] E. Stanewsky. private communication. 1999.

[67] E. Stanewsky, J. J. Thibert. Airfoil SKF 1.1 with maneuver flap. AGARD AR 138, A5-1 - A5-29, 1979.

[68] J. L. Steger, R. F. Warming. Flux Vector Splitting of the Inviscid Gasdynamic Equations with Application to Finite-Differnce Mehtods. *J. Comput. Phys.*, 40: 263–293, 1981.

[69] I. Thomas. Zur Lösung der zweidimensionalen Euler - Gleichungen: Elliptische Netzgenerierung und Finite - Volumen - Verfahren. Diplomarbeit, Hamburg, 1998.

[70] E. F. Toro. *Riemann Solvers and Numerical Methods for Fluid Dynamics.* Springer, Berlin, Heidelberg, New York, 1997.

[71] E. Turkel. Preconditioned Methods for Solving the Incompressible and Low Speed Compressible Equations. *J. Comput. Phys.*, 72: 277–298, 1987.

[72] S. Ukai. The incompressible limit and the initial layer of the compressible Euler equations. *J. Math. Kyoto Univ.*, 26: 323–331, 1986.

[73] H. A. van der Vorst. BI-CGSTAB: A fast and smoothly converging variant of BI-CG for the solution of nonsymmetric linear systems. *SIAM J. Sci. Stat. Comput.*, 13: 631–644, 1992.

[74] B. van Leer. Flux-vector splitting for the Euler equations. In *Eighth International Conference on Numerical Methods in Fluid Dynamics*, (Ed.) E. Krause, number 170 in Lecture Notes in Physics, pp. 507–512, Berlin, 1982. Springer Verlag.

[75] J. Vierendeels, K. Riemslagh, E. Dick. A Multigrid Semi-implicit Line-Method for Viscous Incompressible and Low-Mach-Number Flows on High Aspect Ratio Grids. *J. Comput. Phys.*, 154: 310–341, 1999.

[76] G. Volpe. Performance of Compressible Flow Codes at Low Mach Numbers. *AIAA J.*, 31 (1): 49–56, 1993.

[77] Y. Wada, M.-S. Liou. A Flux Splitting Scheme with High-Resolution and Robustness for Discontinuities. *AIAA Paper*, 94–0083, 1994.

[78] W. Waidmann, F. Alff, M. Böhm, U. Brummund, W. Clauss, M. Oschwald. Supersonic Combustion of Hydrogen/Air in a SCRAMJET Combustion Chamber. *45th Conference of the International Astronautical Federation*, IAF-94-S.4.429, 1994.

[79] J. M. Weiss, W. A. Smith. Preconditioning Applied to Variable and Constant Density Flows. *AIAA J.*, 33 (11): 2050–2057, 1995.

Address: Priv.-Doz. Dr. Andreas Meister, Fachbereich Mathematik, Schwerpunkt Differentialgleichungen und Dynamische Systeme, Universität Hamburg, Bundesstraße 55, 20146 Hamburg, Germany